博士論文

論文題目 Analysis of molecular mechanism of single-membrane-bounded peroxisome dividing ring discovered by genomic science, and the origin of organelles in the view of their division

（ゲノム科学による単膜系ペルオキシソームの分裂リングの発見と分子機構に関する研究、及びそれに基づくオルガネラの起源に関する考察）

氏　　名　　井元　祐太

Acknowledgements

I wish to express my deepest gratitude to Professor Shigeyuki Kawano at University of Tokyo and Professor Tsuneyoshi Kuroiwa at Rikkyo University, for their kind instruction and continuous encouragement throughout this study, as well as their critical reading of the manuscript during the preparation of this thesis, and I also acknowledge with thanks Dr Haruko Kuroiwa at Rikkyo University, for kind instruction and continuous encouragement throughout this study, useful suggestion and discussion. I am extremely grateful to Dr Mio Ohnuma at Rikkyo University for her experimental instruction, and kind instruction to gene engineering of *Cyanidioschyzon merolae* cells, Dr Yamato Yoshida at Michigan State University for his experimental instruction and kind instruction to isolation of organelles from *C. merolae* cells, Dr Takayuki Fujiwara at National institute of Genetics for his experimental instruction and useful discussion about single-membrane-bounded organelle proliferation, Dr Masaki Yoshida at Tsukuba University for his kind instruction to proteomic analysis of *C. merolae*, Dr Osami Misumi at Yamaguchi University, Dr. Shin-ya Miyagishima, Dr Shunsuke Hirooka at National Institute of Genetics, Dr Keiji Nishida at Kobe University for his experimental instruction, Dr Fumi Yagisawa at University of California University and Shinichiro Maruyama at National Institute for Basic Biology for their useful suggestion and discussion, and Mr. Aida at JEOL for kind instructions about apparatus for high-pressure freeze fixation.

I would like to express my deepest appreciation to all members of this laboratory and Professor Kuroiwa's laboratory, Dr Tomokazu Yamazaki, Dr

Contents

Preface

It is generally believed that the cell cycle consists essentially of the mitotic cycle, which involves mitosis and cytokinesis. These processes are becoming increasingly well understood at the molecular level. However, successful cell reproduction requires duplication and segregation (inheritance) of all of the cellular contents, including not only the cell-nuclear genome but also intracellular organelles. Eukaryotic cells contain three types of double-membrane-bounded organelles (cell nucleus, mitochondria and chloroplast) and four types of single-membrane-bounded organelles [endoplasmic reticulum (ER), Golgi body, lysosomes and peroxisomes (Microbodies)]. These seven membrane-bounded organelles cannot be formed de novo and daughter organelles must be inherited from parent organelles during cell cycle.

However, the cells of higher animals and plants contain many organelles which tend to behave somewhat randomly, there is little information concerning the division and inheritance of these double- and single-membrane-bounded organelles. I used the unicellular red alga *Cyanidioschyzon merolae* is a very small organism (1.5–2.0 μm diameter), whose cells offer unique advantages for studies of double- and single-membrane-bounded organelle division cycles. They contain a minimal set of organelles; i.e. a cell nucleus, a mitochondrion, a chloroplast, a peroxisome, an ER, a single Golgi body and a few lysosomes (Matsuzaki et al. 2004; Yagisawa et al. 2007; 2009) (Fig. P-1). Its organelle divisions can be highly synchronized with the light/dark cycle (Suzuki et al. 1994). The genome of *C. merolae* has been completely sequenced and it is one of the smallest genomes (16.5 Mb), with the lowest number of genes among free-living eukaryotes (Matsuzaki et al. 2004; Nozaki et al. 2007). The

genome was not contained myosin gene and actin genes were not expressed (Takahashi et al. 1996). Therefore, cytokinesis occurs in the absence of the contractile rings, but EF1α has been located in the contractile ring region, and it is likely that this protein controls cytokinesis in many eukaryotic cells (Imoto et al. 2011a; 2011b). Because most of the genes are present in low copy numbers and lack introns, they are suitable for identifying gene and protein functions by post genomics using microarray, matrix assisted laser desorption ionization time of flight mass spectrometry (MALDI-TOF-MS) and gene engineering.

Besides studies of the mitotic cycle, mitochondrial division and chloroplast division behavior have been examined by using *C. merolae*. Mitochondria and chloroplast arose from an endosymbiotic bacterial ancestor and have their own genomes that are maintained by division (Margulis, 1970; Kuroiwa, 1982; Gillham, 1994; Cavalier-Smith, 2000; Miyagishima et al. 2003b). Function and the components of mitochondrial division (MD) machinery and chloroplast (plastid) division (PD) machinery have been revealed by microarray analysis of its gene expression profile during organelle division (Fujiwara et al. 2009), MALDI-TOF-MS (Yoshida et al. 2006; 2009; 2010) and gene targeting (Ohnuma et al. 2009; Yoshida et al. 2013). The MD machinery was composed of the inner machinery (inner MD ring, FtsZ1, ZED) and the outer machinery (outer MD ring, Dnm1, Mda1) (Nishida et al. 2003; 2007, Yoshida et al. 2009). The PD machinery was composed of the inner machinery (inner PD ring, FtsZ2) and the outer machinery (outer PD ring, Dnm2, PDR1) (Miyagishima et al. 2003; Yoshida et al. 2010), and outer machinery was bundle of PDR1-mediated polyglucan filaments (Yoshida et al. 2010).

2

The behavior and inheritance of single-membrane-bounded organelles is related to their metabolic processes (Fig. P-2). mRNA is synthesized in the cell nucleus and moves to the ER for translation. Proteins are transported from the ER to the Golgi body, which processes and packages both proteins and lipids. Subsequently, these processes are aided by the activities of lysosomes and peroxisomes. Therefore, the localization of these organelles is intimately related to their function established in their early evolution. In *C. merolae*, the cell nuclear division during mitosis is accompanied by the inheritance of the ER and Golgi body in association with the microtubules and spindle poles (Yagisawa et al. 2012; 2013). By contrast, lysosomes and peroxisomes function as more or less independently from the synthetic function of the cell nucleus, the division (inheritance) of these organelles is not directly related to the division of cell nuclei but to the division of mitochondria (Miyagishima et al. 1999b; Yagisawa et al. 2007). The functions of lysosomes and peroxisomes suggest that the origins of these organelles during eukaryotic evolution may have been later than those of the ER and Golgi body (Kuroiwa et al. 2008).

During the M phase, lysosomes and peroxisomes were physically attached to mitochondria and inheritance (division and segregation) of these organelles is accompanied by mitochondrial division and segregation (Miyagishima et al. 1999b; Yagisawa et al. 2007). Inheritance of lysosomes was revealed by microarray analysis and immunological assays of *C. merolae*. It was mediated by a 30-kDa coiled-coil protein, vacuole inheritance gene 1 (VIG1) which tethered the lysosomes to the daughter mitochondria by constructing net-like structures (Fujiwara et al. 2010).

Inheritance of peroxisome occurred during mitochondrial segregation in *C. merolae* (Miyagishima et al. 1999b; Imoto et al. 2011a). However, the structure of the machinery involved in the division and segregation of peroxisomes has not been identified. This has been one of the enigmatic problems in cell biology ever since the discovery of peroxisome by Rohdin and de Duve (Rohdin 1954; de Duve 1969). As the cells of multi-peroxisomal organisms, such as yeasts, plants, and animals, contain irregularly shaped peroxisomes that divide randomly, their inheritance has been examined by analyzing peroxisome abundance and distribution (Tabak et al. 2003; Koch et al. 2003). Therefore, the machinery that is essential for inheritance and plays a central role was unclear. The aim of this study was to elucidate the structure and function of the mechanochemical machinery involved in peroxisome inheritance using *C. merolae.*

  This thesis consists of two parts. First (Chapter 1), inheritance of peroxisomes and mitochondria mediated by spindle poles in the primitive red alga *C. merolae.* Observations of microtubule dynamics during the division cycles showed that spindle poles are fundamentally important for segregation of the mitochondrion. In addition, peroxisome division and segregation was controlled by progression of mitochondrial segregation via spindle poles. Second (Chapter 2), Single-membrane–bounded peroxisome division revealed by isolation of dynamin-based machinery. Dynamin-related protein 3 (DRP3) ortholog, CmDnm1 (Dnm1) predominantly accumulated with catalase in the isolated dividing-peroxisome fraction. Dnm1 formed a ring at the division site of the peroxisome. Immunoelectron microscopy revealed that the ring was the

peroxisome-dividing (POD) machinery which consists of two different structures. In addition, differences between single- and double-membrane–bounded organelle division machineries were examined, giving insight into the origin of organelles in the view of their division.
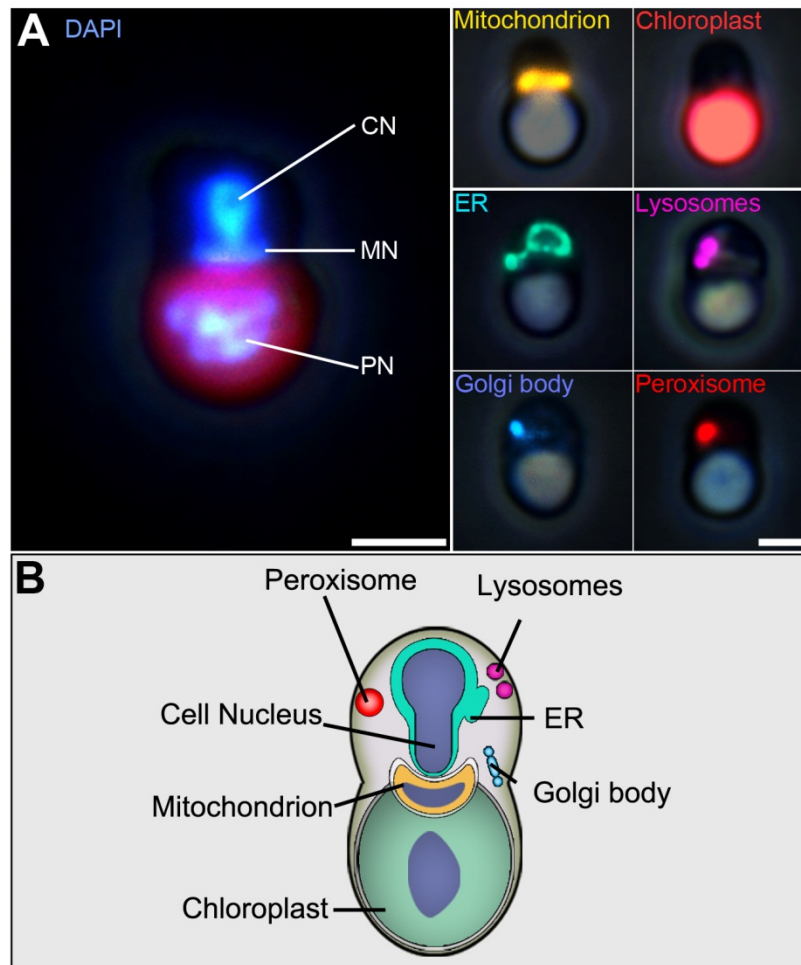
Fig. P-1. The red alga *Cyanidioschyzon merolae* as a tool for studying organelle proliferations.

(A) Phase contrast DAPI staining images of *C. merolae* shows localization of DNA of cell nucleus (CN), mitochondrial (MN) and chloroplast (plastid) (PN). Phase contrast immunofluorescence images show mitochondrion (yellow; anti-POR), chloroplast (autofluorescence), ER (cyan; anti-calnexin), Golgi body (light blue; anti-Sed5), lysosomes (purple; anti-V-ATPase) and peroxisome (red; anti-catalase). *C. merolae* is small (2μm in diameter), unicellular organism that inhabits sulphate-rich hot springs (pH 1.5-2.5, 45°C). (B) The schematic interphase cell contains a cell nucleus, one mitochondrion, one chloroplast, one ER, one Golgi body, two or three lysosomes, one peroxisome and lacks a rigid cell wall.
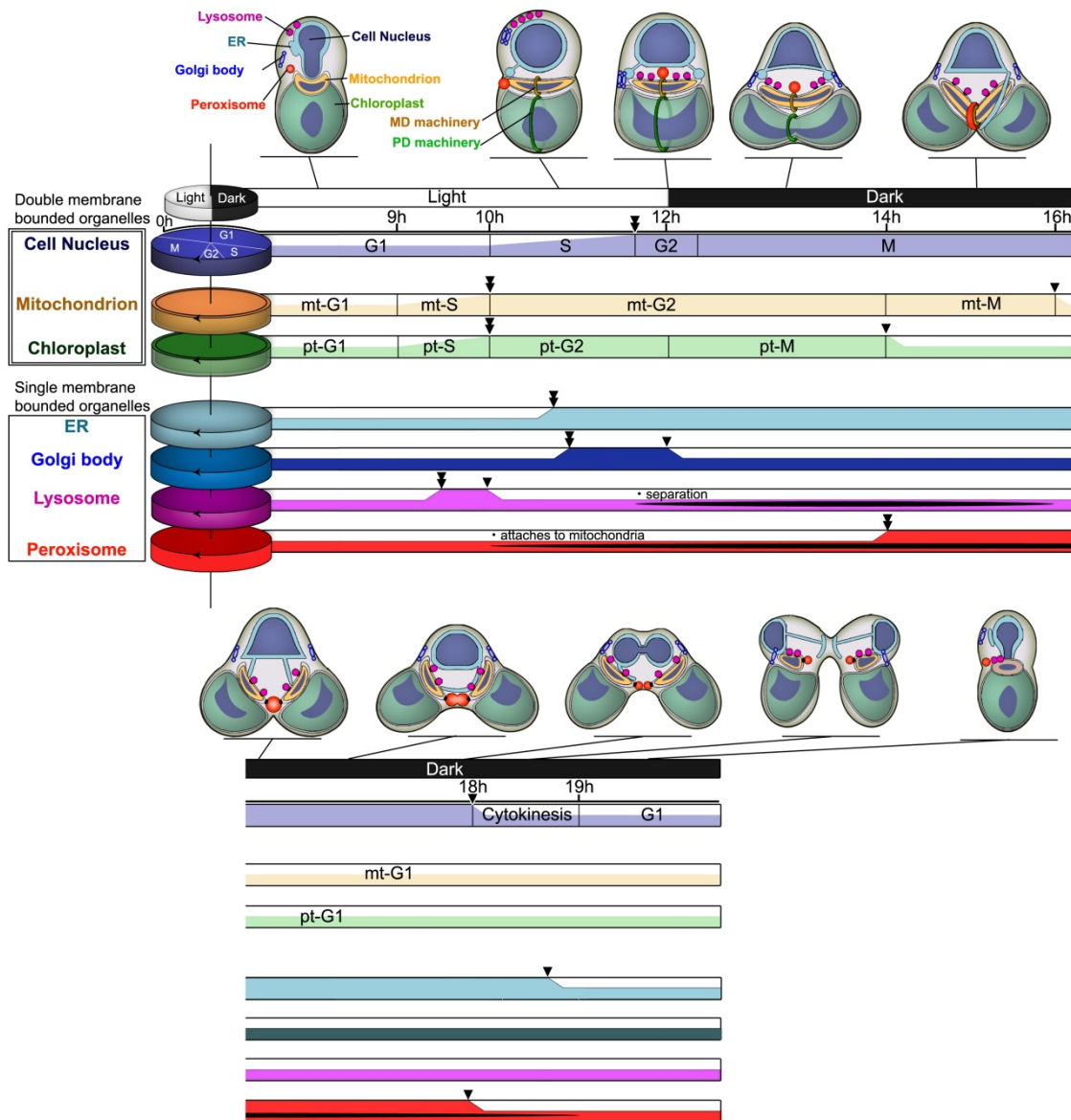
Fig. P-2. Summary of the division cycles and the temporal relationships of the three double-membrane-bounded organelles and the four single-membrane-bounded organelles in *C. merolae* cells.

Chloroplast and mitochondrion divide using the PD and MD machineries, respectively. Peroxisome and lysosome are inherited using the mitochondrion as a carrier. Double arrowheads indicate the time point of the organelle replication and single arrowheads indicate the time point of the organelle division. Time shows hours after the second cell cycle of synchronization.

7

Chapter 1

Inheritance of peroxisomes and mitochondria mediated by spindle poles in the primitive red alga *Cyanidioschyzon merolae*

Abstract

Cells proliferate by duplicating their contents and dividing. The cycle of duplication and division is called the cell cycle, and the events of the cell cycle are generally understood as the mitotic cycle. However, the cell contains other double membrane-bound organelles (mitochondria and chloroplast) and single membrane-bound organelles (endoplasmic reticulum, Golgi body, lysosome peroxisome). Plant and animal cells contain many organelles which divide randomly; therefore, it has been difficult to elucidate these organelle proliferations. In this study, immunofluorescence analysis using α-tubulin, porin and catalase antiserum revealed that spindle poles and microtubules control inheritance of mitochondrion and peroxisome during the late mitotic (M) phase. I used the primitive red alga *Cyanidioschyzon merolae*, as it contains a single mitochondrion and peroxisome per cell, and organelle division can be synchronized by a light/dark cycle. I demonstrated that chloroplast, mitochondria and peroxisome multiplied by independent division cycles and divided in this order. Division of mitochondria and chloroplast occurred during G2 – early M phase, while division of peroxisome occurred during late M phase 2 hours after the mitochondrial division. Although peroxisome divided into two daughter peroxisomes by binary fission as same as the division of mitochondrion and chloroplast, putative electron dense peroxisome-dividing rings were not identified at the division

sites by thin section electron microscopy after chemical fixation. However, the inheritance of peroxisome and mitochondrion was found to be dependent on microtubules as well as cell–nuclear division. I have observed five stages of microtubule dynamics: (1) the microtubule disappears during the G1 phase; (2) α-tubulin is dispersed within the cytoplasm without forming microtubules during the S phase; (3) α-tubulin is assembled into spindle poles during the G2 phase; (4) polar microtubules are organized along the mitochondrion during prophase; and (5) mitotic spindles in cell nuclei are organized during the late M phase and spindle poles attached to the edges of daughter mitochondria. During the late M phase, both edges of dividing peroxisome were attached to daughter peroxisomes. Inhibition of microtubule organization induced cell–nuclear division, daughter mitochondria segregation, and delay of peroxisomal division during the late M phase, suggesting that similar to cell–nuclear division, inheritance of peroxisome and mitochondrion dependent on microtubules.

Introduction

  Eukaryotic cells contain at least three types of double membrane-bound organelles [cell nucleus, mitochondrion and chloroplasts (plastids), and four types of single membrane-bound organelles [endoplasmic reticulum (ER), Golgi body, lysosomes (vacuoles) and peroxisome (microbody)]. These membrane-bounded organelles cannot be formed de novo but are inherited by growth, division and separation during cell cycle. The double -membrane-bounded organelle plays a role as a leading apparatus of the inheritance (division and separation) of the single-membrane-bounded

organelles (Kuroiwa et al. 2008; Imoto et al. 2011a). The cell-nucleus divides accompanied by ER and Golgi body (Yagisawa et al. 2012; 2013), while the mitochondria divide accompanied by a peroxisome and lysosomes (Miyagishima et al. 1999; Yagisawa et al. 2007; Fujiwara et al. 2010). Therefore, to understand the proliferations of these seven double- and single-membrane-bounded organelles, we need to recognize not only how the mitotic cycle takes place but also how these organelle division cycles occur. These semiautonomous characteristics led to the concept of the "mitochondria division cycle," as proposed by Kuroiwa et al. (1978). In the slime mold *Physarum polycephalum*, the mitotic and mitochondrial division cycles were examined, as the mitotic cycle is naturally synchronized and the mitochondria contain large rod-shaped mitochondrial nuclei (a complex of DNA and proteins known as nucleoids). The results showed that each phase such as mitochondrial (mt) S, mtG2, mtM, and mtG1 of the mitochondrial division cycle differed remarkably from that of the mitotic cycle (Kuroiwa et al. 1978). Similar results were obtained in cultured tobacco BY2 cells, but mtS, mtM, chloroplast (cp) S, and the ptM phase could not be identified (Yasuda et al. 1988). Many researchers have investigated the timing of synthesis of mitochondrial DNA (mtDNA) during the cell cycle and have shown that timing of the mtS phase varies, depending on the species. Synthesis of mtDNA has been observed to occur during the S phase of the mitotic cycle, from the late S phase to the G2 phase, during other phases of the mitotic cycle, or even throughout the mitotic cycle as summarized by Itoh et al. (1997). The links among the mitotic cycle, mitochondrial division cycle, chloroplast division cycle, and peroxisome division cycle are poorly understood. This poor understanding is due to the fact that, in slime molds, higher plants and animals: cells

contain a large number of organelles; the morphology of organelles such as mitochondria and chloroplasts is generally complex and variable, and it is difficult to discriminate between dividing organelles and nondividing organelles; the organelles divide randomly during the cell cycle; and the organelles move in entire cells. I used the primitive red alga *Cyanidioschyzon merolae*, which contains a cell nucleus, a mitochondrion, and a chloroplast per cell, to study organelle division cycles as it can be highly synchronized via a light/dark cycle. The cpM and mtM phases were identified during the cell cycle by observing organelles after staining with 4′,6-diamidino-2- phenylindole (DAPI; Kuroiwa et al. 1995). Itoh et al. (1997) suggested relationships between the mitotic cycle and chloroplast, mitochondrial, and peroxisome division cycles in the alga using electron microscopy. To elucidate the relationship between the mitotic cycle and organelle division cycles, the DNA contents in each organelle accompanying the morphological change of organelles must be examined throughout the cell cycle. Additionally, the dynamics of cytoskeletal proteins, which play a major role in the cell transport system and division during the mitotic cycle, must be scrutinized during the cell cycle. Higher eukaryotes contain complicated microtubule systems and a greater number of organelles, whereas in *C. merolae*, two actin genes are not expressed (Takahashi et al. 1996; Matsuzaki et al. 2004), the myosin gene is absent (Suzuki et al. 1995), and five kinesin motor proteins are expressed (Matsuzaki et al. 2004). Microtubules are only organized to form spindles during mitosis (Nishida et al. 2005). These unique systems in primitive eukaryotes suggest that the cytoskeletal or transport systems seen in higher eukaryotes were acquired courtesy of evolutionary processes, and then diverged from the mitotic apparatus in early eukaryotes. Microtubules are

fundamentally important for cell nuclear and organelle division. *C. merolae* serves as a model system to study the general mechanisms of cell nucleus and organelle–nucleus proliferation. In the present study, I characterized the relationships between the mitotic, mitochondrial division, chloroplast division, and peroxisome division cycles. I also demonstrated mitochondrial and peroxisome divisions and mitosis by microtubules that was mediated by spindle poles using microfluorometry and cytochemical techniques.

Results

Synchronization of cell nucleus, mitochondrial, and chloroplast divisions

To identify each phase of the mitotic, mitochondrial division, and plastid division cycles during the *C. merolae* cell cycle, cell division was synchronized according to methods described previously (Fujiwara et al. 2009a). The DNA content in cell nuclei, mitochondria, and plastids were examined by VIMPCS after staining with DAPI. Fig. 1-1A shows typical interphase and mitotic cells fixed at 2 and 18 h, respectively, after the initiation of synchronization. Interphase cells contained one cell nucleus, one mitochondrion, and one chloroplast whereas mitotic cells contained dividing or divided cell nuclei, mitochondria, and chloroplasts. The cell nuclei, mt-nucleoids (mt-nuclei), and chloroplast-nuclei (cp-nucleoids) emitted white–blue fluorescence, and chloroplast emitted red autofluorescence. In the mitotic cells, the cell nuclei, mt-nuclei, and cp-nuclei were stretched toward both cell poles. Fig. 1-1B contains representative micrographs of type I–XII cells arranged in order of

divisional progress with the results summarized in Fig. 1-2. The type I cell contained a spherical cell nucleus inserted into the mitochondrion and a cup-shaped plastid. The type II cell contained a spherical cell nucleus, flat mitochondrion, and spherical plastid with spherical cp-nucleus. The type III cell contained a spherical and larger cell nucleus than the type II cell. Chloroplast structure was rectangular, and its bottom was flat. Both ends of the upper part of the dumbbell-shaped cp-nucleus were stretched toward both upper ends of the chloroplasts as if the end of the cp-nucleus was associated with the membrane. In the type IV cell, the cell nucleus appeared hat shaped, and the mt-nucleus was wider than the type III cells and stretched toward both poles of the cell. The chloroplast was more rectangular than type III cells, and cp-nucleus was segregating with both ends stretched toward both poles of the mt-nuclear structure. In the type V cell, the chloroplast was dividing, and the mt-nucleus formed a triangle-shaped structure, with both ends of the mt-nucleus stretched toward both ends of the daughter mitochondria. Both ends of the dividing cell nucleus, mitochondrion, and chloroplast coincided with both spindle pole areas (Fig. 1-1B). In the type VI cell, the mt-nucleus formed a V-shaped structure, and the chloroplast divided into daughter plastids. In type VII cells, the mitochondrion and the plastid divided into daughter organelles. The type VIII cells contained a condensed cell nucleus following chloroplast and mitochondrial divisions. Daughter chloroplasts and mitochondria were separated completely, and individual chromosomes were not visible. The stretched end of the upper part of the cp-nucleus could be seen in daughter chloroplasts. The type IX cell contained one dividing dumbbell-shaped cell nucleus, daughter mitochondria, and daughter chloroplasts. The individual chromosomes in the daughter cells

13

were not observed. The type X cell contained daughter cell nuclei, mitochondria, and chloroplasts in the dividing cell. The type XI cell contained daughter cell nuclei, mitochondria, and chloroplasts, and a cleavage furrow for cytokinesis began to appear at the equator of the cell. The type XII cell contained daughter cell nuclei, mitochondria, and chloroplasts, in which these organelles were separated from each other and cytokinesis had occurred.

To determine the G1, S, G2, and mitotic phases of the cell nucleus, mtG1, mtS, mtG2, and mtM phases of mitochondria and cpG1, cpS, cpG2, and cpM phases of chloroplasts during cell cycle, DNA content of each cell nucleus, mt-nucleus, and cp-nucleus was examined directly using VIMPCS after staining with DAPI (Fig. 1-1C). Microfluorometry analysis showed changes in the DNA content per cell nucleus, mitochondrion, and chloroplast at various times following the initiation of cell culture synchronization. The ratio of cell–nuclear DNA content doubled from 10 to 12 h following the commencement of synchronization with the cell–nuclear S phase occurring during these 2 h. The ratio decreased half during from 16 to 18 h. Since the ratio of dividing, dumbbell-shaped cell nuclei began to increase from 12 to 14 h, and the G2 phase of cell nuclei was less than 1 h and around 12 h after initiation of the second light period. The mitosis was about 6 h, and then, cytokinesis occurred from 18 to 20 h, and the cell entered the G1 phase (Fig. 1-1C and D). From the cell number counted during the one set of second period of the synchronization(Fig. 1-1D) and the first period of the synchronization described in a previous study (Fujiwara et al. 2009a), the duration of the cell cycle was determined to be 22 h. I determined the duration of each phase in the mitotic cycle with the S phase at 2 h, G2 was less than 1 h, and the M phase was 8 h long; therefore,

14

the G1 phase was determined to be approximately 12 h. The method used to determine each phase of the mitotic cycle was applied to determine each phase of the mitochondrial and chloroplast division cycles with the results summarized in Fig. 1-2 and Table 1-1. The cpS phase of the plastid division cycle and the cpS phase of the mitochondrial division cycle preceded approximately 1 h before the S phase of the mitotic cycle. The division of the plastid was completed first followed by the mitochondria and then finally by the cell nuclei. I were also able to identify the duration of each phase of the mitochondrial (mtG1, 15 h; mtS 1 h; mtG2, 4 h; mtM, 2 h) and chloroplast division cycles (cpG1, 17 h; cpS, 1 h; cpG2, 2 h; cpM, 2 h). The results clearly demonstrated that the cell cycle could be understood not only by the mitotic cycle but also by mitochondrial and chloroplast division cycles.

Divisions of mitochondrion and peroxisome during the cell cycle

The time difference between the mtS, cpM, and M phases during organelle division cycles and mitotic cycles is very useful in demonstrating the organelle and mitotic division. Previously, 3-dimentional analysis by using transmission electron microscopic images showed that peroxisome touches the mitochondrion via electron-dense structure during the division of mitochondrion and peroxisome (Miyagishima et al. 1999b). Therefore, mitochondrion is thought to be the leading apparatus of the inheritance of the peroxisome (Miyagishima et al. 1999b; Kuroiwa et al. 2008; Imoto et al. 2011a). To investigate the mechanism of inheritance of mitochondrion and peroxisome, immunofluorescence microscopy analysis against synchronized *C. merolae cells* by using anti-porin antibodies and

anti-catalase antibodies during cell cycle were performed (Fig. 1-3). Peroxisome was localized in cytosol during the G1 phase and attached to mitochondria during M phases. After mitochondrial division during the prophase (early M phase), oval-shaped peroxisomes become dumbbell-shaped and finally divide into two daughter peroxisomes by binary fission during the metaphase to the telophase (late M phase). Fig. 1-4 shows electron microscopic images of three serial sections of the same cell. The daughter chloroplasts became full of thylakoid membranes associated with a large amount of phycobilisomes, while a small peroxisome about 200 nm in diameter appears to be dumbbell-shaped. Although peroxisome divided into two daughter peroxisomes, putative electron dense structure was not identified at the division site after the chemical fixation.

Protein levels of α-tubulin during the cell cycle

As the electron-dense structure was not observed at the peroxisomal division site after the chemical fixation, another mechanism which regulates the inheritance of the peroxisome was investigated. Previous study showed that microtubules were involved in mitochondrial proliferation (Nishida et al. 2005), I investigated the roles of microtubules in peroxisome proliferation. *C. merolae* cells were synchronized and harvested every 2 h for 24 h after initiation of the second light period. Immunoblotting analysis of α-tubulin showed that it appeared during the S phase and existed throughout the M phase (Fig. 1-5A). Protein levels of α-tubulin were quantified using VIMPCS and compared with transcription levels of α-tubulin obtained by microarray analyses (Fig. 1-5B). The

transcription levels of α-tubulin were increased between late G1 and G2 phase, reaching a peak during prophase then decreasing during metaphase. Synthesis of α-tubulin occurred approximately 2 h after transcription of RNA and continued during the G2 and M phases.

Characterization of microtubule organization throughout the cell cycle

To characterize the microtubule dynamics throughout the cell cycle, cells at various phases of the cell cycle were examined by immunofluorescence microscopy after triple staining with anti-α-tubulin antibody (tubulin), DAPI (DNA), and anti-POR antibody (mitochondria). Fig. 1-6 demonstrates α-tubulin staining during the S, G2, and M phases. During the G1 phase, signals corresponding to the presence α-tubulin were not seen. The α-tubulin proteins evident during the S phase just after synthesis were probably monomers and were located throughout the entire cytoplasm, then organized to form spindle poles at each end of the mitochondrion and cell nucleus during the G2 phase. During the early M phase, the bridge-like tubulin between bipolar spindle poles appeared along the mitochondrion and transformed into a V-shaped structure, accommodating the change in shape of the dividing mitochondrion (mitochondrial polar microtubules). However, microtubules were not apparent on the chloroplast. The V-shaped tubulin structure separated to form spindle poles at each end of the cell nucleus. During the late M phase, a central bridge between spindle poles at each end of the cell nucleus formed and extended. These results suggested that microtubule dynamics during the cell cycle are separated into several specific stages: (1) microtubules are not organized during the G1 phase; (2) α-tubulin is synthesized and dispersed in the cytoplasm during the S phase;

17

(3) α- tubulin accumulated to form spindle poles during the G2 phase; (4) microtubules were organized along the mitochondria during the organelle division period; and (5) a central spindle bridge between spindle poles is organized during the M phase.

Role of microtubules in mitochondrial and peroxisomal inheritance

To investigate the role of microtubules in mitochondrial, chloroplast and peroxisomal inheritance, synchronized cells were treated with oryzalin, an inhibitor of microtubule organization. Following treatment, the α-tubulin in cells during the M phase did not organize to form microtubules and spindle poles, and was dispersed throughout the cytoplasm as in S phase cells (Fig. 1-7A). At 20 h after the initiation of the second light period, almost all the cell nuclear divisions were arrested, and the mitochondria had divided but not separated, while chloroplast had divided (Fig. 1-7A and B), whereas peroxisome had divided (Fig. 1-8). Because the peroxisomes divide within a very short time (Miyagishima et al. 1999a), few dividing peroxisomes were detected, even during late M phase in control cells (Fig. 1-8B). Although peroxisome fission was occurred after the oryzalin treatment, frequency of the dividing peroxisomes was increased from 18 h to 24 h after the one set of the synchronization (Fig. 1-8B). This result indicating that velocity of the peroxisomal division was slow in the oryzalin treated cells and completion of the division was delayed.

Discussion

Cell–nuclear and organelle DNA dynamics during cell cycle

18

It is difficult to identify each phase of the mitochondrial, chloroplast, and organelle division cycles in plant and animal cells due to the following reasons: (1) cells contain a large number of organelles; (2) the morphology of organelles such as mitochondria and chloroplasts is complex and variable, and thus difficult to discriminate between dividing and nondividing organelles; (3) organelles divide randomly during the cell cycle; (4) organelles contain a small amount of DNA; and (5) the organelles move within the cells (Yasuda et al. 1988). Therefore, I used the primitive red alga *C. merolae* to study organelle division cycles due to its relative simplicity and ability to be synchronized by a light/dark cycle. Previous work has demonstrated the existence of a mitotic cycle as well as mitochondrial, chloroplast, and peroxisomal division cycles in *C. merolae* cells using cytological and morphological techniques (Suzuki et al. 1994; Kuroiwa et al. 1995; Itoh et al. 1997; Miyagishima et al. 1999a; Fujiwara et al. 2009a). However, I could not identify all phases and their durations of the various cycles. Therefore, I examined the DNA content in each organelle of synchronized cells by VIMPCS after staining with DAPI to identify all phases and their durations. Similar to the cell nuclei, mitochondria and chloroplast s undergo essential processes such as DNA replication, organelle–nuclear (nucleoid) division, and organelle division (organelle kinesis). One division cycle of cell nuclei, mitochondria, and chloroplasts lasts approximately 22 h. DNA synthesis and division of chloroplasts and mitochondria precede cell–nuclear division. Previous studies revealed that organelle DNA replication always occurs before cell–nuclear DNA replication (Sakai et al. 2004). The results presented here suggest that there is also organelle to cell nucleus regulation during the M

phase.

Inheritance of the peroxisome during the late M phase

Peroxisomes are spherules, 0.5–2.0 μm in diameter, and are characterized by the presence of the enzyme catalase, which protects the cell from oxidative stress, such as that caused by peroxide produced following the exposure of cellular metabolites to high concentrations of molecular oxygen (De Duve and Baudhuin 1966). Peroxisomes play a role in β-oxidation of fatty acids. They are present in a wide variety of eukaryotic lineages, including Archeplastida, Excavata, Amoebozoa, and Opisthokonta (Gabaldón et al. 2006). The number of peroxisomes ranges from 1 per cell in primitive organisms like *C. merolae* to between 10 and 400 per cell in Archeplastida and Opisthokonta (Brown et al. 1983; Gray and Iglesia 1984; Miyagishima et al. 1998). For proper function and inheritance of eukaryotic cells, the number of peroxisomes needs to be maintained (Tabak et al. 2003; Koch et al. 2003). There have been many investigations into the mechanism of proliferations of peroxisomes. In the animal and the plant cells, peroxisomes proliferate by division (Koch et al. 2003; Fujimoto et al. 2008). In the yeast cells, peroxisomes are generated from domains in the ER (Hoepfner et al. 2005). However, it was difficult to clarify the mechanisms of inheritance of peroxisomes due to the cells of plant and animal contain a large number of peroxisomes which divide randomly. Therefore I used *C. merolae* which contains a single peroxisome. After the light/dark synchronization, immunofluorescence microscopy using anti-catalase antibodies showed that peroxisome divide by binary fission during the late M phase after the mitochondrial division and distributed to

daughter cells evenly (Fig. 1-3). Previously, Miyagishima et al. (1999a) showed that volume of peroxisome is duplicated in early M phase. These current and previous studies suggest that peroxisome basically proliferate by division.

Effects of inhibiting microtubule organization

 I was able to clarify various stages of microtubule dynamics involved in the inheritance of mitochondrion and peroxisome using the antibodies against α-tubulin of *C. merolae*. These microtubule dynamics could be classified into five specific stages as follows: (1) microtubules were not organized during the G1 phase; (2) α-tubulin was synthesized but dispersed in the cytoplasm during the S phase; (3) α-tubulin form spindle poles during the G2 phase; (4) polar microtubules were formed along the mitochondrion during the mtM phase; and (5) a central mitotic spindle between spindle poles formed within the cell nucleus during the M phase. The last point is not conflict with the previous study (Nishida et al. 2005). In general, microtubules were always organized during the cell cycle and played a major role in cytoskeletal transport and spindle formation during cell division. Our results demonstrated that there are no cytoskeletal transport systems around the cytoplasm during the cell cycle, especially in the G1 and S phases of primitive *C. merolae* cells (Fig. 1-6).

 After oryzalin treatment, microtubules throughout the M phase cells were dispersed within the cytoplasm, much like cells in the S phase. This supports the idea that microtubules were not organized during the S phase but dispersed without polymerization. Generally, cytoskeletal microtubules are involved in organelle movement or morphology, mitochondrial

positioning in higher plants (Van Gestel et al. 2002) and peroxisome movement in mammals (Wiemer et al. 1997), while microtubules during the M phase are involved in division of the cell nucleus. However, in *C. merolae*, cells in the G1 and S phase clearly demonstrated that there were no cytoskeletal microtubules present. In a previous study, following oryzalin treatment, mitochondria were able to divide using mitochondrial division machinery but failed to segregation (Nishida et al. 2005). During the segregation, spindle poles and the both edges of daughter mitochondria were connected by using microtubule-like structures (Nishida et al. 2005). In this study, the α-tubulin in cells during the M phase was not able to organize and form microtubules between the spindle poles, instead remaining dispersed within the cytoplasm after the oryzalin treatment (Fig. 1-7A). Therefore, microtubules and spindle poles are important for mitochondrial segregation. In addition, velocity of peroxisome division was low after the oryzalin treatment (Fig. 1-8). Previous study showed that electron dense patch-like structures were observed between the daughter mitochondria and both edges of dividing peroxisome (Miyagishima et al. 1998b). This structure may involve in binding the peroxisome to the mitochondrion, and in division and segregating daughter peroxisomes. In *C. merolae*, these results suggest that division of peroxisome is controlled by spindle poles and microtubules via daughter mitochondria. Although completion of peroxisome division was delayed without spindle poles and microtubules, peroxisome fission occurred correctly. Therefore, another mechanism involved in peroxisome division is required in addition to the spindle poles and microtubules. Electron-dense structures were not observed at the division sites of dumbbell-shaped peroxisome after the chemical fixed three serial sections (Fig. 1-4). Furthermore, lines of

evidence required to clarify mechanisms of peroxisome division by other techniques.

Material and methods

Synchronous culture and drug treatment

C. merolae strain 10D-14 (Toda et al. 1998) was used, and the cells were cultured and synchronized as previously described (Suzuki et al. 1994) with minor modification. For synchronization, the cell culture was maintained in $2\times$ Allen's medium at pH 2.8 subjected to continuous light (40 W/m^2) and shaking at 40°C. The cells were subcultured to yield a concentration of $1\times$ 10^7 cells per milliliter and subjected to 3 h of darkness, and were then synchronized on a 12-h light/12-h dark cycle at 40°C while the medium was aerated. Experiments with synchronized cultures commenced from the second light period. For oryzalin treatment, a 1/2,500 volume of 100 mM oryzalin stock solution dissolved in dimethyl sulfoxide was added 8 h following the commencement of synchronization. For observation of DNA, cell fixation was performed as follow. Each sample were collected after the centrifugation, and subjected to the fixation buffer {2% v/v glutaraldehyde in TAN buffer [17% (w/v) sucrose, 20 mM Tris-HCl (pH 7.6), 0.5 mM EDTA, 1.2 mM sper- midine, 7 mM 2-mercaptoethanol and 0.4 mM PMSF]} on ice for 30 min. Images were viewed using an epifluorescence microscope (BX51; Olympus, Japan) with a 3CCD digital camera (C7780; Hamamatsu Photonics, Japan) utilizing ultraviolet excitation. The intensity of fluorescence of DAPI-stained DNA was quantified using a video-intensified microscope photon-counting system (VIMPCS), as

described previously (Kuroiwa et al. 1986).

Antibodies

Mouse anti-α-tubulin antisera had been characterized previously (Fujiwara et al. 2009b). Immunoblotting was performed by applying 20 μg of a total protein extract from *C. merolae* and separated on 12.5% sodium dodecyl sulfate–polyacrylamide gels, then transferred onto polyvinylidene difluoride membranes. After blocking with 5% skim milk in Triton X-100 Tris-buffered saline (TTBS), the membranes were incubated with anti-α-tubulin antisera at a dilution of 1:1,000 in TTBS. Alkaline phosphatase-conjugated goat antimouse IgG was used at a dilution of 1/1000 as the secondary antibody. Signals were detected using an alkaline phosphatase (AP) conjugate substrate kit (Bio-Rad, USA) and quantified via VIMPCS. The transcription level of α-tubulin during the cell cycle was defined according to a microarray analyzed in a previous study (Fujiwara et al. 2009a).

Microscopy

Cell fixation and immunofluorescence microscopy were performed as described previously (Nishida et al. 2004). Primary and secondary antibodies were used at the following concentrations: 1:500 for mouse anti-α-tubulin antiserum, 1:1,000 for Alexa-488 goat anti-mouse antibody, 1:1,000 for guinea pig anti-mitochondrial Porin (POR) antiserum: a mitochondrial marker protein (Fujiwara et al. 2009b), 1:1000 for Alexa-555 goat anti-guinea pig antibody, 1:1000 for rabbit anti-CENH3 antiserum: a

1:1000 for Alexa-555 goat anti-rabbit antibody, 1:1,000 for rat anti-catalase antiserum: a peroxisome marker protein (Ohnuma et al. 2009), and 1:1,000 for Alexa-555 goat anti-rat antibody.

Chemical fixation for electron microscopy

  Synchronized cells were collected by centrifugation and fixed in 0.4% w/v glutaraldehyde in 2x Allen's medium and then washed in 10 mM cacodylate buffer. Then the samples were fixed in 1% OsO_4 for overnight at 4°C and dehydrated throughout series of ethanol dehydration and embedded in Spurr's resin (Yagisawa et al. 2009).

Microfluorometry

  The intensity of fluorescence was quantified using a VIMPCS as described previously (Kuroiwa et al. 1986) with minor modifications. The relative DNA copy number in the cell nucleus, mitochondrion, and chloroplast were calculated based on the intensity of DAPI-stained DNA content at each sampling time, normalized to the DNA content at the initiation of synchronization (G1 phase). Intensity measurement was done for irregular shaped areas of cell nuclei, mitochondria, and plastids.

Table. 1-1 Duration of the mitotic phases of the cell nucleus, mitochondrion
and plastid in *C. merolae* determined by DNA contents and morphology

Cell cycle phases	Estimated average duration in hours		
	Cell nucleus	Mitochondrion	Chloroplast
G1	12	15	17
S	2	1	1
G2	~1	4	2
M	8	2	2
Cell cycle	22	22	22
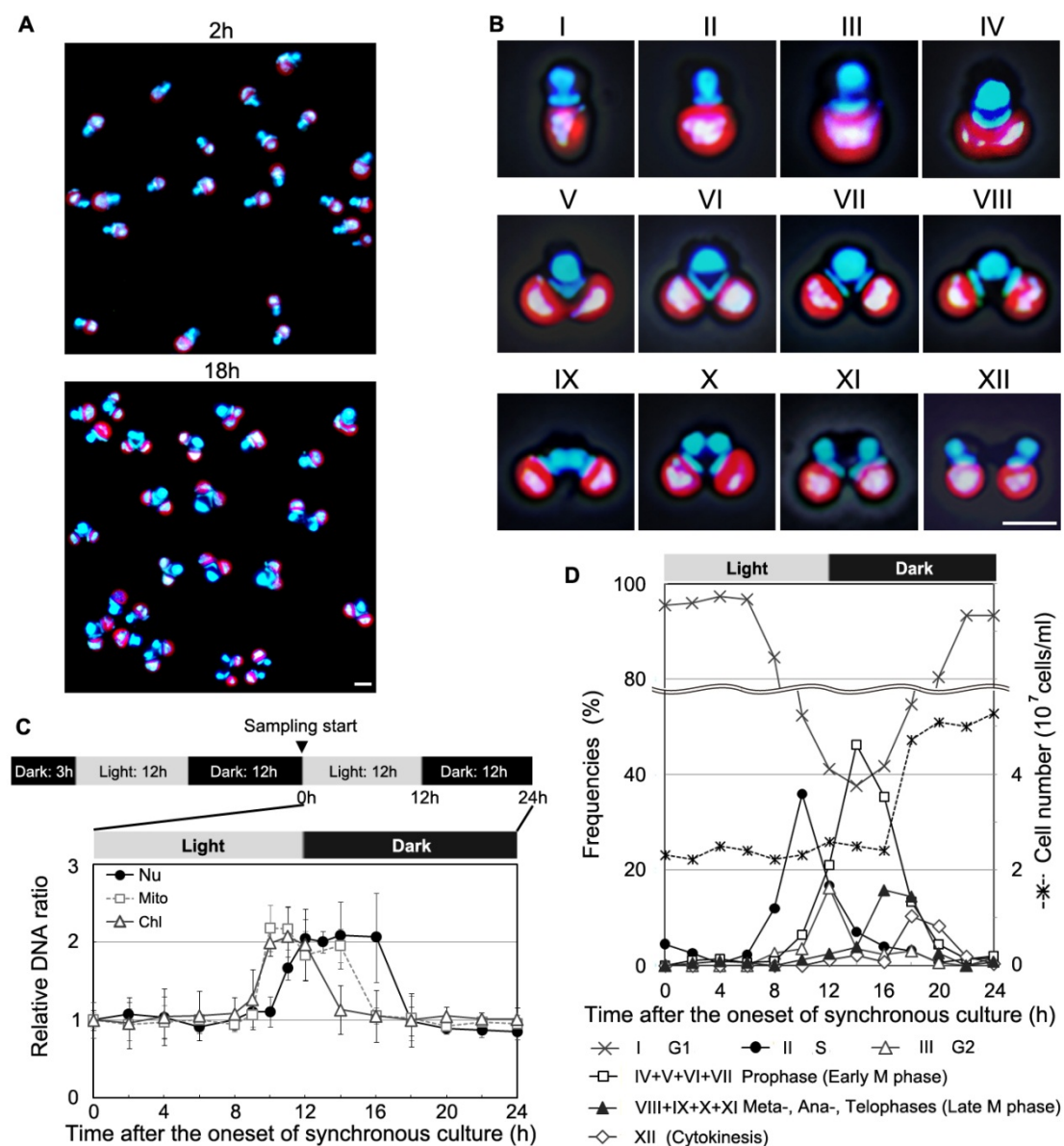
Fig. 1-1. Synchronous culture and definition of the cell cycle phases of *C. merolae.*

(A) Images of synchronized interphase (2 h) and mitotic (18 h) cells. (B) DAPI-stained images of type I–XII cells observed through mitotic phases. (C) Dynamics of contents of the cell nucleus (Nu), mt-nucleus (Mito), and chl-nucleus (Chl) throughout the cell cycle. DNA content was measured by VIMPCS and expressed as relative copy numbers normalized to the state of initiation of synchronized cells (means ± SD, n=10). (D) Frequencies of type I–XII cells and changes in cell number. Scale bars: 2 μm.
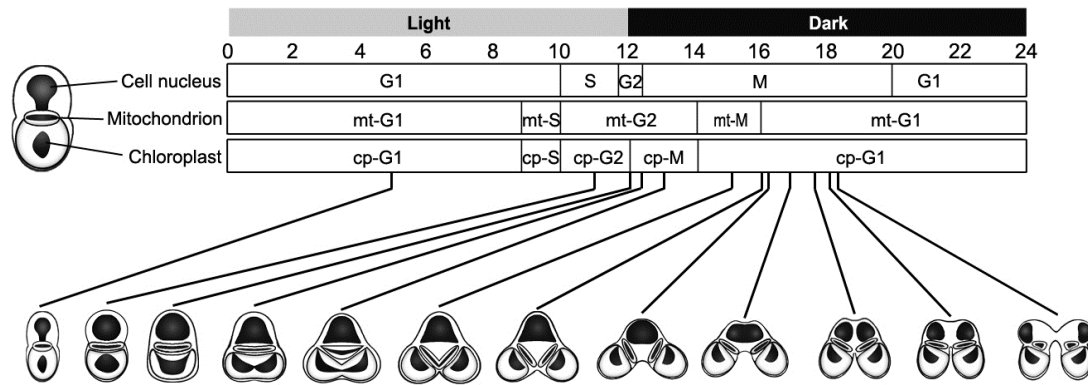
Fig. 1-2. Summary of the temporal relationship between cell–nuclear, mitochondrial, and plastid division cycles.

Bars indicate mitotic cycle: G1, S, G2, M (cell nucleus mitotic phases: prophase, metaphase, anaphase, telophase, cytokinesis); mitochondrial division cycle: mitochondrial G1 phase (mt-G1), mitochondrial S phase (mt-S), mitochondrial mitotic phase (mt-M); and plastid cell cycle: chloroplast G1 phase (cp-G1), plastid S phase (cp-S), plastid mitotic phase (cp-M).Type I–XII cells are illustrated in the cell cycle order.
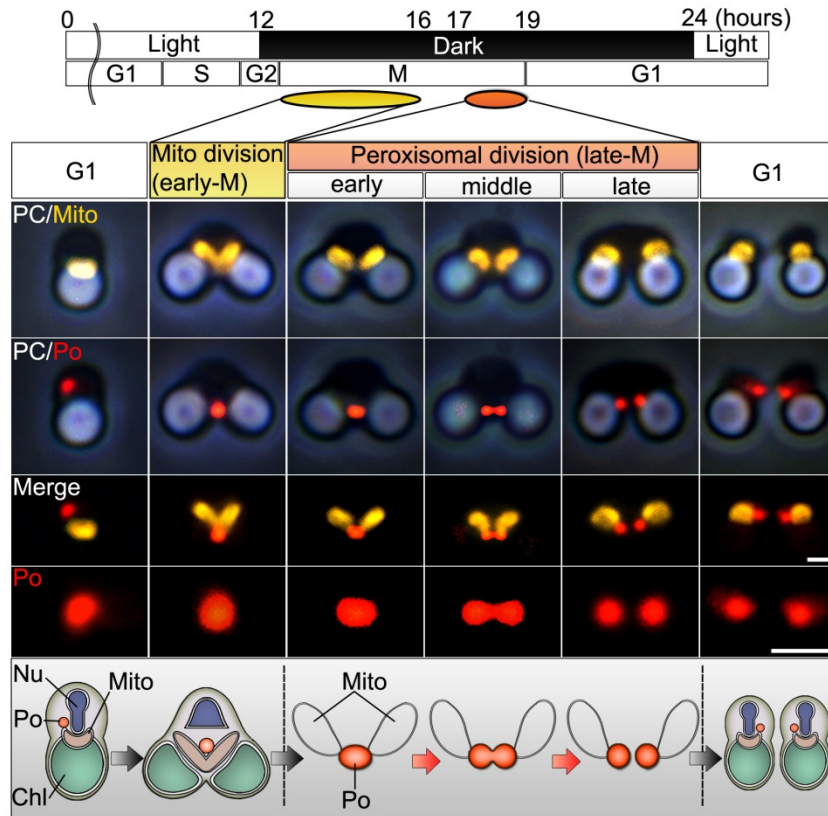
Fig. 1-3. Proliferations of mitochondrion and peroxisome during the cell cycle.

Immunofluorescence and schematic images of mitochondrial and peroxisomal divisions of *C. merolae*. Peroxisome (red) division occurred after mitochondrial (yellow) division. Chl, chloroplast; Mt, mitochondrion; Nu, cell nucleus; PC, phasecontrast image; Po, peroxisome. Scale bar: 1 μm.
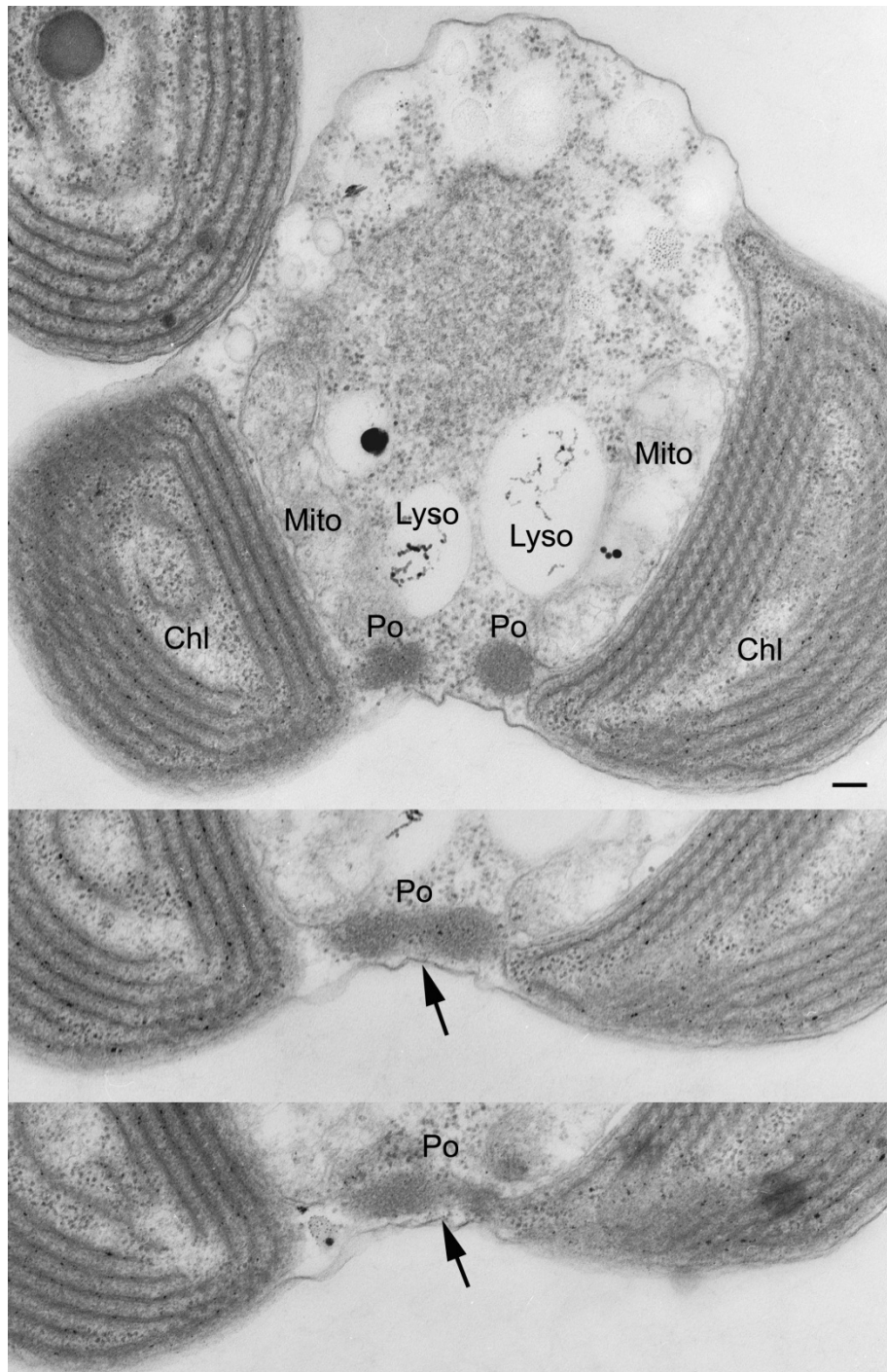
Fig. 1-4. Serial microscopic images of three serial section showing double-membrane bounded organelles and dividing peroxisome.

  After chemical fixation, electron dense structure was not visualized at division site (arrow). Scale bar: 100 nm. Po, peroxisome; Lyso, Lysosome; Mito, mitochondria; Chl, chloroplast.
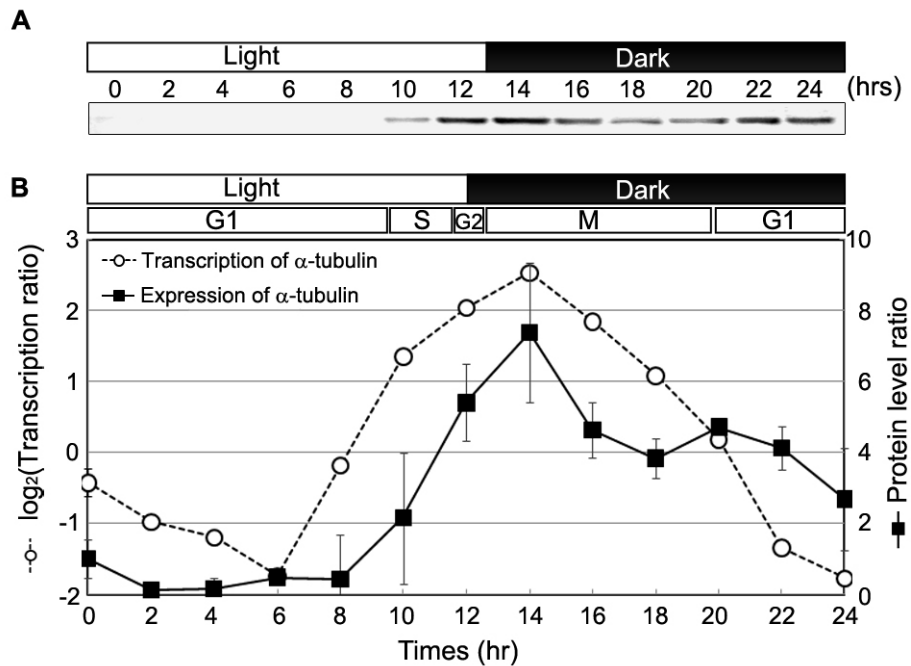
Fig. 1-5. Transcription and protein levels of α-tubulin.

(A) Immunoblotting analysis of α-tubulin throughout the cell cycle. Cells were harvested at the indicated time points after the initiation of synchronization. Twenty micrograms of total protein was loaded, and α-tubulin was detected using mouse α-tubulin antiserum of *C. merolae*. (B) Relationship between the ratio of the transcription levels of α-tubulin and the ratio of α-tubulin protein levels. The protein level was normalized to the intensity of the band at initiation of cell synchronization (0 h). Mean ± SD; n=3
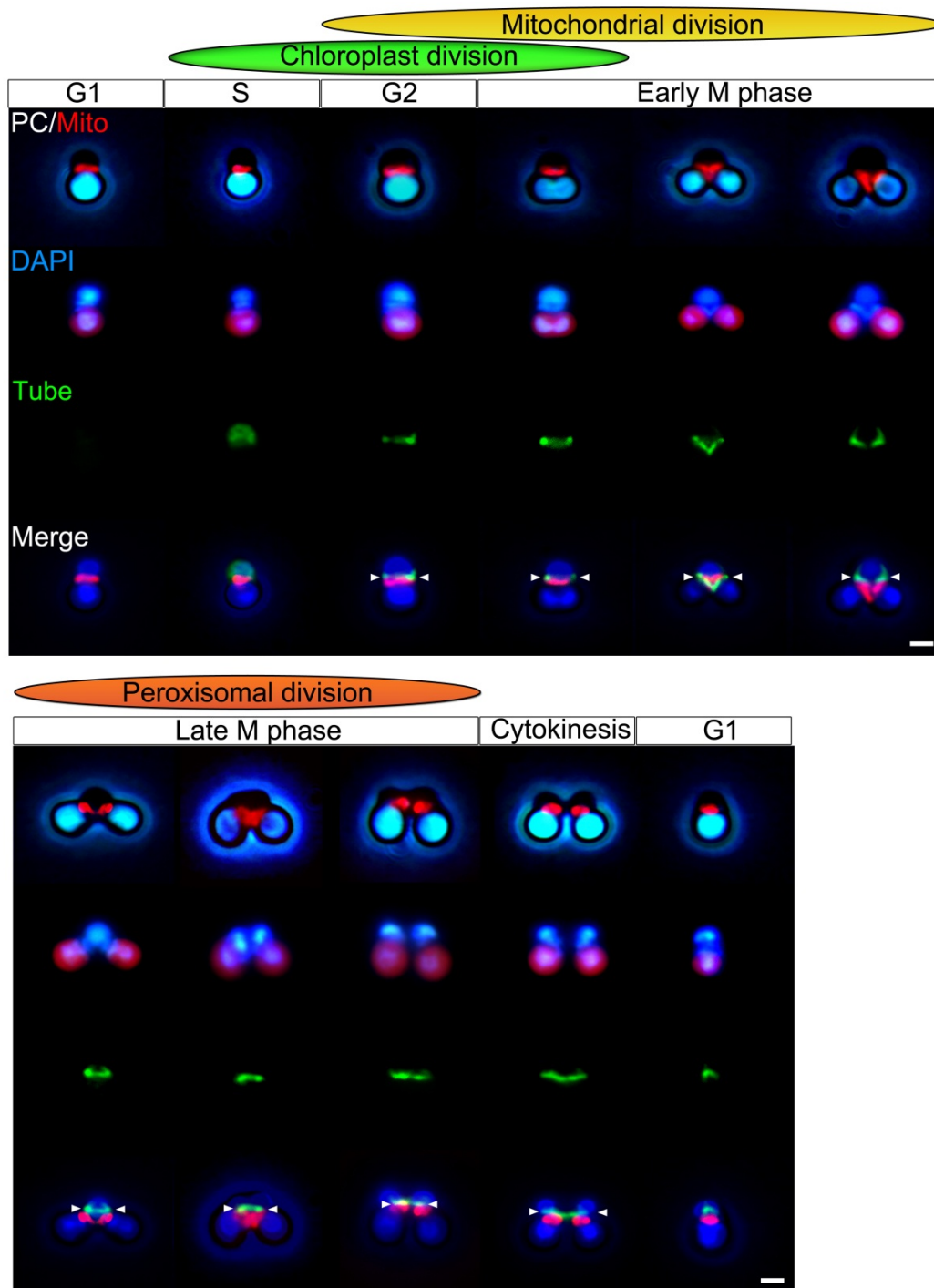
Fig. 1-6. Microtubule dynamics in *C. merolae*.

Immunofluorescence of microtubules, mitochondria. Images of cells fixed and immunostained for microtubules (green), mitochondria (red), and DNA (blue) according to the predicted order of the cell cycle. Arrowheads indicate spindle poles. Scale bar: 1 μm.
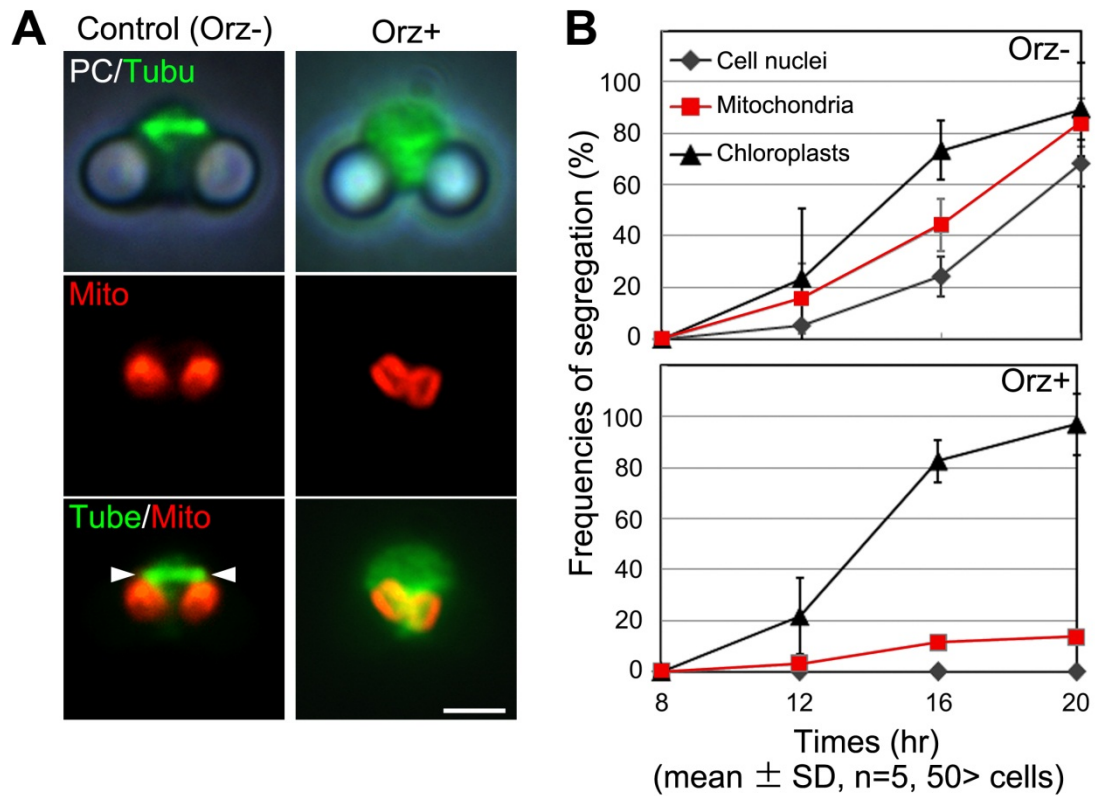
Fig. 1-7. Effects of inhibiting microtubule organization on the mitochondria division.

(A) Oryzalin effects on mitochondrial segregation. Cells were fixed and immunostained to visualize mitochondria and microtubules. (B) Oryzalin effects on the segregated organelles in synchronous culture. Scale bar 1 μm. Arrowheads indicate spindle poles. Mean ± SD, n=5, 50> cells.
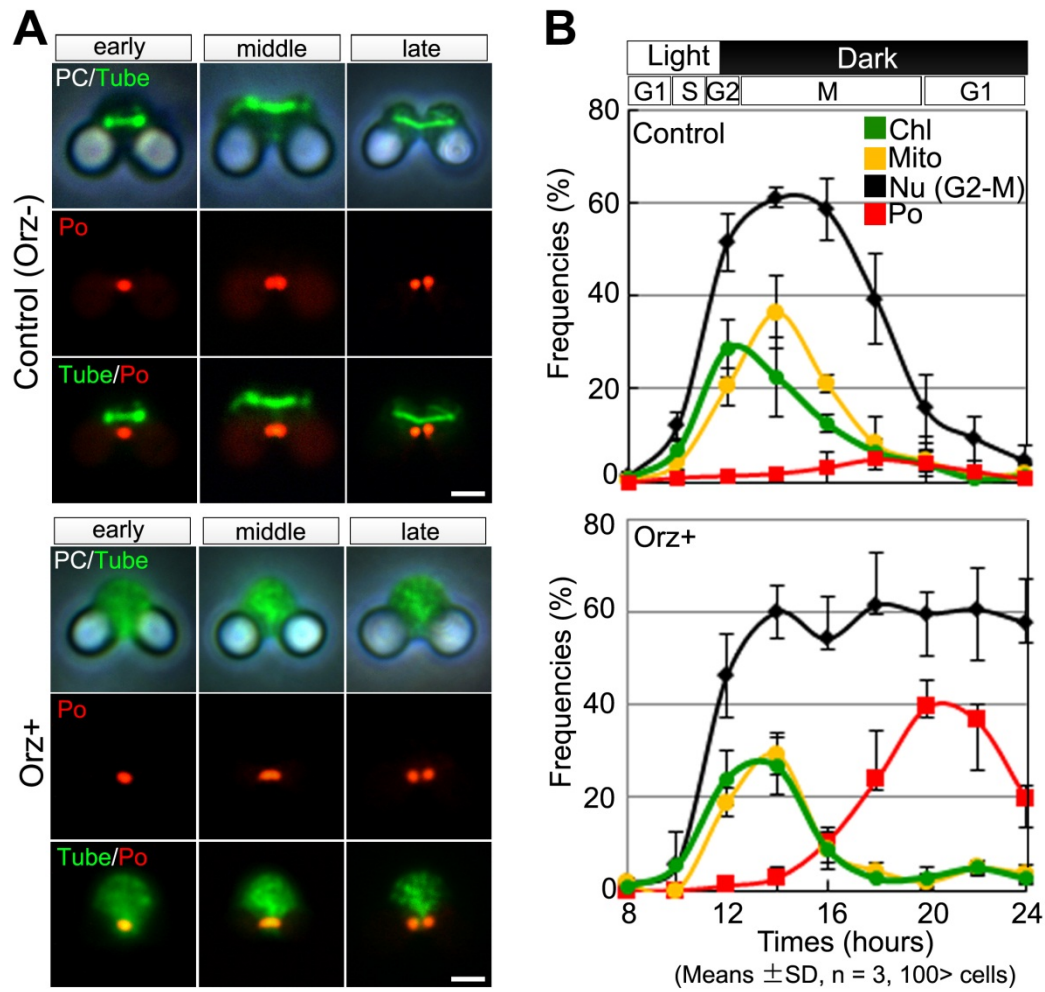
Fig. 1-8. Effects of inhibiting microtubule organization on the peroxisome division.

(A) Oryzalin effects during the peroxisome division period. Cells were fixed and immunostained to visualize peroxisome and microtubules. (B) Frequencies of dividing organelles in synchronous culture before and after the oryzalin treatment. Scale bar 1 μm. Mean ± SD, n=3, 100> cells.

Chapter 2

Single-membrane–bounded peroxisome division revealed by isolation of dynamin-based machinery

Abstract

Peroxisomes are ubiquitous single-membrane–bounded organelles and fulfill essential roles in the cellular metabolism. They are found in virtually all eukaryotic cells and basically multiply by division. However, the mechanochemical machinery involved in peroxisome division remains elusive. Here, I first identified the peroxisome-dividing (POD) machinery. I isolated the POD machinery from *Cyanidioschyzon merolae*, a unicellular red alga containing a single peroxisome. Peroxisomal division in *C. merolae* can be highly synchronized by light/dark cycles and the microtubule disrupting agent oryzalin. By proteomic analysis based on the complete genome sequence of *C. merolae*, I identified a dynamin- related protein 3 (DRP3) ortholog, CmDnm1 (Dnm1), that predominantly accumulated with catalase in the dividing-peroxisome fraction. Immunofluorescence microscopy demonstrated that Dnm1 formed a ring at the division site of the peroxisome. The outlines of the isolated dynamin rings were dimly observed by phase contrast microscopy and clearly stained for Dnm1. Electron microscopy revealed that the POD machinery was formed at the cytoplasmic side of the equator. Immunoelectron microscopy showed that the POD machinery consisted of an outer dynamin-based ring and an inner filamentous ring. Down-regulation of Dnm1 impaired peroxisomal division. Surprisingly, the same Dnm1 serially controlled peroxisomal division after mitochondrial division. Because

genetic deficiencies of Dnm1 orthologs in multiperoxisomal organisms inhibited both mitochondrial and peroxisomal proliferation, it is thought that peroxisomal division by contraction of a dynamin-based machinery is universal among eukaryotes. These findings are useful for understanding the fundamental systems in eukaryotic cells.

Introduction

Peroxisomes are single-membrane–bounded organelles found in nearly all eukaryotic cells. In plant cells, peroxisomes are involved in a variety of metabolic pathways essential for development associated with photorespiration, lipid mobilization and hormone biosynthesis (Schrader and Yoon 2007; Pan and Hu 2011). In animals, abnormalities in peroxisome proliferation are associated with carcinogenesis, neurodegeneration, and cerebrohepatorenal syndrome (Schrader and Yoon 2007; Gould and Valle 2000). Peroxisomes are thought to basically proliferate by division, although they do not contain DNA (Schrader and Yoon 2007). Because the cells of multiperoxisomal organisms, such as yeasts, plants, and animals, contain irregularly shaped peroxisomes that divide randomly, their proliferation has been examined by analyzing peroxisome abundance and distribution (Koch et al. 2004; Motley and Hettema 2007). Therefore, the division machinery (ring) that is essential for proliferation and plays a central role is unclear. *Cyanidioschyzon merolae* offers unique advantages for studying peroxisomal division, because each cell contains a minimal set of basic eukaryotic organelles, comprising one chloroplast, one mitochondrion, one cell nucleus, and one peroxisome, the divisions of which occur in that order and can be synchronized by light/dark cycles

36

(Miyagishima et al. 1999a, 1999b; Imoto et al. 2010) (Fig. 2-1). In *C. merolae*, peroxisomes do not form de novo from the endoplasmic reticulum in the peroxisomal division cycle but divide by binary fission (Miyagishima et al. 1999a; Kuroiwa et al. 2008).

This chapter describes the structure and function of POD machinery. For the purpose, we performed isolation of dividing peroxisomes from *C. merolae* cells. POD machinery consisted of dynamin-based (DB) ring and Filamentous ring. DB ring was string including dynamin which generates motive force for contraction and encircled filamentous ring. Filamentous ring was circular structure and partially disassembled during the contraction. Thus, single-membrane-bounded peroxisome divided by the contraction of POD machinery.

Results

Proteomic analysis of isolated dividing peroxisomes

To search for proteins essential for peroxisomal division, I developed a protocol to isolate dividing peroxisomes and analyzed them by MALDI-TOF-MS. I developed a method to collect cells containing dividing peroxisomes by oryzalin treatment (Fig. 1-8). This resulted in the temporary accumulation of cells containing dividing peroxisomes. Cells were harvested at 12 h after the oryzalin treatment and were lysed in a French Pressure Cell. During the peroxisomal division period, dividing peroxisome is attached to daughter mitochondria via electron-dense patches (50 nm in diameter) (Miyagishima et al. 1999). Therefore, dividing peroxisome, daughter mitochondria and daughter chloroplasts were isolated

as organelle complex (Fig. 2-2A). Daughter mitochondria and daughter chloroplasts were lysed with non-ionic detergent and hypotonic treatment, and dividing peroxisomes were isolated (Fig. 2-2B). Isolated peroxisomal fractions were examined by MALDI-TOF-MS. As a result, proteins in 10 (control cells) and 13 (oryzalin-treated cells) bands were identified (Fig. 2-3, Table 2-1). The major subtracting bands included catalase and CmDnm1/DRP3 (Dnm1). Dnm1 is one of only two dynamins (Dnm1 and Dnm2) encoded in the *C. merolae* genome (7, 11). Dnm1 and Dnm2 are important components of the MD machinery (16, 17) and PD machinery (16, 17), respectively. Immunoblot analysis indicated that Dnm1 was concentrated in the dividing-peroxisome fraction with catalase (Fig. 2-4), suggesting the interesting possibility that same Dnm1 serially controls peroxisomal division after mitochondrial division.

Subcellular localization of Dnm1

mRNA of Dnm1 was constantly expressed through the cell cycle, while mRNA of Dnm2 was specifically expressed during the chloroplast division suggested that Dnm1 has multi functions besides mitochondrial division (Fig. 2-5). Immunofluorescence microscopy showed that Dnm1 signals appeared as cytoplasmic patches (dynamin patches) in G1 phase cells and localized at the mitochondrial division site in early M phase cells as described in previous study (Nishida et al. 2003) (Fig. 2-6). Dnm1 signal was observed through cell cycle and Dnm1 localized to the peroxisomal division site at 1.5 h after mitochondrial division (Fig. 2-7). During the mitochondrial division or peroxisomal division, signal intensities of Dnm1 decreased in the cytosol and increased at the mitochondrial division site or

peroxisomal division site. After the mitochondrial division or peroxisomal division, signal intensities of Dnm1 increased in the cytosol (Fig. 2-8). These results suggested that there were dynamic recruitments of Dnm1 to between dynamin patches and the mitochondrial or peroxisomal division sites. In slightly squashed oryzalin-treated and control cells, I observed dynamin ring-like structures encircling the equator of dividing peroxisomes (Fig. 2-9). The diameter of the dynamin ring decreased as the diameter of the division site decreased during peroxisomal division (Fig. 2-10), suggesting that the dynamin ring has a role in contraction at the division site.

Isolation of dynamin rings

  Immunofluorescence microscopy and immuno-EM revealed that isolated dividing peroxisome visualized by whole-mount EM were swollen compared to immunofluorescence microscopy and Dnm1 was localized on the bridge between the isolated daughter peroxisomes (Fig. 2-11). When the bulk peroxisomal contents were dissolved using membrane dissolution buffer, isolated dynamin rings were clearly observed by immunostaining for Dnm1. The outlines of the dynamin rings were dimly visible by phase-contrast microscopy (Fig. 2-12A). The dynamin rings were not stained for the antibodies against mitochondrial-division apparatus 1 (Mda1), filamentous-tempreture sensitive Z1 (FtsZ1) or plastid-dividing ring 1 (PDR1) (Fig. 2-12B). SDS/PAGE and MALDI-TOF-MS analyses showed that the Dnm1 band was concentrated in the insoluble fraction (Fig. 2-12C). The width of the dynamin ring increased as peroxisomal division progressed, but the total fluorescence intensity of the ring did not change

(Fig. 2-12D). These findings suggested that the peroxisome divides by contraction of the dynamin ring formed at an early period. When the membrane was partially dissolved by detergent, skeletal filamentous rings appeared (Fig. 2-13A, B) with peroxisome membrane, which was labeled with catalase (Fig. 2-13C and Table 2-2). These consisted of a bundle of fine filaments of 4–5 nm in diameter (Fig. 2-14).

Composition of the POD machinery

An in vitro guanosine triphosphatase (GTPase) assay did not induce a conformational change in the dynamin rings isolated from dividing peroxisomes (Fig. 2-15). This finding can be explained by considering the structural analogy to the PD machinery, in which motive force for the contraction of the putative ring working together in addition to the GTPase activity of dynamin molecules (Yoshida et al. 2006).

To clarify the structure involved in the contraction of dynamin ring of peroxisome, isolated dynamin rings were observed using immunoelectron microscopy. Dnm1-bound immunogold particles (yellow arrowheads) were arranged at distances of about 10–20 nm along the skeletal filamentous structure (Fig. 2-16). Dynamin localized on strings peeled away from the skeletal filamentous ring, suggesting that the peroxisome-dividing (POD) machinery consisted of the dynamin-based (DB) ring (a complex of dynamin and amorphous string) and the filamentous ring (Fig. 2-17A-C). The DB ring branched from the filamentous ring showed a string and part of the ring formed a clump (Fig. 2-17D and E), while the filamentous rings were remained as smooth curve (Fig. 2-17D-F). These results suggest that the DB ring has motive force for the contraction of filamentous ring.

Electron dense structure of POD machinery with thin section

  Although structure of the isolated POD machinery was observed by immunofluorescence and immunoelectron microscopy, putative electron dense ring of POD machinery were not identified at the division sites in sections (Chapter 1 Fig. 1-1). Then I used high-pressure freeze fixation apparatus for fixation of *C. merolae* cells. Figure 2-18 shows electron microscopic images showing daughter peroxisomes during late period of peroxisomal division after high-pressure freeze fixation. The football shaped peroxisome became dumbbell shaped, and divided into 2 daughter peroxisomes of equal size by binary fission. A thin belt-like structure about 20 nm in width, surrounding the constricted site, was faintly visualized in detailed observations of the bridge between daughter peroxisomes (Fig. 2-18A). In addition, just before pinching off of daughter peroxisomes, electron dense peroxisome-dividing rings of about 200 nm in diameter were observed in the perpendicular image to the division plane (Fig. 2-18B). The peroxisome-dividing ring is much smaller in size and weaker in density than MD and PD rings (Miyagishima et al. 1999a). These results suggest that peroxisome divides by contraction of electron dense ring.

  Comparisons between the POD machinery and the MD/PD machineries

  To understand the mechanisms of the POD machinery, structures of the POD machinery were compared with the PD and MD machinery. The isolated POD machinery and the isolated PD machinery formed circular shaped, while the isolated MD machinery formed irregularly shaped and

difficult to examine morphological feature (Fig. 2-19A). Dnm1-bound immunogold particles were localized at a distance of 10–30 nm from the outer periphery of the POD machinery (Fig. 2-19C). Dnm2-bound immunogold particles were localized are closely attached to the peripheral region of the PD machinery before contraction and moved to inside when diameter of the ring become smaller (Fig. 2-19D). The isolated POD machineries were circular structure throughout contraction but the isolated PD machineries could form super-twisted structure (Fig. 2-20). The width of filamentous ring was smaller than PD machinery and remained constant during contraction, whereas those of isolated PD machinery increased (Fig. 2-21). At the late stage of contraction, the filamentous ring appeared to be resolved, leaving only the DB ring (Fig. 2-22). These observations suggested that the contraction of the POD machinery was caused by the DB ring containing Dnm1 and the filamentous ring accompanied by partial disassembly.

Down-Regulation of Dnm1 during peroxisomal and mitochondrial division

To investigate the role of dynamin in the POD machinery during peroxisomal division, I down-regulated Dnm1 using an antisense technique. The antisense-Dnm1 DNA was introduced into cells in non-synchronized culture using a polyethylene glycol method. The frequency of M phase cells increased after the introduction of the antisense-Dnm1 DNA (Fig. 2-23A). The transformed M phase cells with down-regulated Dnm1 showed decreased signal intensity for Dnm1 (Fig. 2-23B) and inhibition of mitochondrial division during early M phase (Fig. 2-23C and D). In

addition, peroxisomal division, which occurred during late M phase, was inhibited and non-dividing peroxisomes were accumulated (Fig. 2-23E and F). In these cells, the dynamin ring did not appear and the peroxisomes became oval shaped (Fig. 2-23G and H). These findings supported the notion that Dnm1 plays an important role in the contraction of the POD machinery, in addition to its role in mitochondrial division.

Discussion

Dual targeting of Dnm1 to the division site of mitochondria and peroxisome

Dynamins are eukaryotic specific families of GTPase that are involved in diverse activities, including endocytosis, Golgi vesicle formation, organelle division and organelle membrane fusion (Praefcke and McMahon 2004). In general, dynamin family members are phylogenetically grouped into eight subfamilies, each of which has one function (Miyagishima et al. 2009). In this study, I showed that dynamin-like protein Dnm1 involved in peroxisome division during late M phase in *C. merolae* (Figs. 2-7 and 2-23). Previously, Nishida et al. (2003) showed that Dnm1 was involved in mitochondrial division during early M phase in *C. merolae*. Molecular genetic studies of animal, fungi and land plants have suggested that dynamin-like protein DRP3, the ortholog of Dnm1, is involved in both mitochondrial division (Bleazard et al. 1999) and peroxisomal proliferation (Li and Gould 2003; Koch et al. 2004; Kuravi et al. 2006; Tanaka et al. 2006; Schrader and Yoon 2007; Fujimoto et al. 2009). Therefore, dual function of Dnm1 family member is conserved in eukaryotic cells.

Microarray analysis showed that Dnm1 was continuously transcribed during the cell cycle while Dnm2 was specifically transcribed during the chloroplast division period (Fig. 2-5). Microfluorometry analysis showed that Dnm1 localized sequentially in the order: cytosol, mitochondrial division site, cytosol, peroxisomal division site and cytosol (Fig. 2-8). These results suggest that Dnm1 recruitment to the division site is not under the regulation of the cell cycle progression but under the regulation of unknown adaptor proteins specific to the division site of mitochondrion or peroxisome. In animal cells, Dnm1 interact with mitochondrial fission 1 (Fis1) in vitro (Kobayashi et al. 2007). Fis1 is transmembrane protein localized at the mitochondrial outer membrane and peroxisomal single-membrane, and involved in both mitochondria and peroxisomes division (Koch et al. 2005; Zhang and Hu 2008). Fis1-like protein is also encoded in *C. merolae genome* (Matsuzaki et al. 2004; Nozaki et al. 2007). However, Dnm1 recruitment to the division sites of mitochondrion and peroxisome were independent of each other in *C. merolae* (Fig. 2-6, Fig. 2-7 and Fig. 2-8). Therefore, another factor which can recruit Dnm1 in distinction from mitochondrial outer membrane and peroxisomal membrane is required. From the perspective of structure of the division machinery, Dnm1 localization was different between the POD machinery and the MD machinery. In the POD machinery, Dnm1 localized on the DB ring which consisted of amorphous string and peeled away from the filamentous ring (Fig. 2-17). In the MD machinery, DB ring like structure was not observed and was considered that Dnm1 closely localized between the fine filaments as well as Dnm2 in the PD machinery (Nishida et al. 2003; Yoshida et al. 2009). Further analysis of components of DB ring is the key to understand the dynamin recruitment to the division site of

mitochondria and peroxisomes.

Function of the POD machinery and comparison between the POD machinery and the MD/PD machineries

To discuss the mechanisms of peroxisomal division, the POD machinery was compared with the MD and PD machineries (Table 2-3). There were at least five differences between single- and double-membrane–bounded organelle divisions. First, the width and diameter of the POD machinery were smaller than those of the MD and PD machineries. Second, the POD machinery lacked bacterium-derived dividing proteins such as FtsZ (Fig. 2-4 and Fig. 2-12B) but contained dynamin derived from host eukaryotes. Therefore, division of the single-membrane–bounded peroxisome may not require the formation of an inner ring on the matrix side. Third, although the MD and POD machineries both contain Dnm1, the isolated POD machinery contains a rigid filamentous ring like the isolated PD machinery but unlike the isolated MD machinery, which forms an irregularly shaped, clumped ring. Whereas the filamentous ring in the PD machinery consists of a bundle of PDR1-mediated polyglucans (Yoshida et al. 2010), the POD machinery did not contain PDR1 (Fig. 2-4 and 2-12). The components of the filamentous ring remain to be identified. Fourth, the isolated POD machinery did not form a supertwisted structure, whereas the isolated PD machinery did (Fig. 2-20). Fifth, the width of the filamentous ring in the POD machinery remained constant during peroxisome contraction, whereas those of the PD machineries increased during contraction (Fig. 2-21). I suggest that dynamin functions in three steps in the operation of the POD machinery (Fig. 2-24). First, Dnm1 molecules form a ring on the cytosolic

side of the outer filamentous ring from cytoplasmic patches during the early period of peroxisomal division. Second, the dynamin-based ring becomes wider, and the filamentous ring partially disassembles during the contraction of the POD machinery. In the PD machinery, the dynamin molecules generate a contraction force by sliding the filamentous ring (Yoshida et al. 2006). In the POD machinery, down-regulation of Dnm1 inhibited the peroxisome contraction, suggesting that the dynamin-based ring generates the motive force for contraction, as well as the POD machinery. Finally, the DB ring directly pinches off the single membrane of the bridge between the daughter peroxisomes after disassembly of the filamentous ring. The divided peroxisomes are separated into daughter cells by electron-dense connectors linking the peroxisomes and mitochondria (Miyagishima et al. 1999b; Kuroiwa et al. 2008).

Origin of peroxisome in the view of their division

The origin of peroxisome has been discussed since the identifications of the structure and function (Rohdin 1954; de Duve 1969). There have been three ideas for the origin of the peroxisome: 1) Peroxisome originates from ER by budding (Tabak et al. 2003; Hoepfner et al. 2005) [Fig. 2-25 Peroxisome (1)], 2) peroxisome evolved from an endosymbiont at the early stage of the evolution of the eukaryotic cell (De Duve and Baudhuin 1966; De Duve 1995) [Fig. 2-25 Peroxisome (2)], and 3) peroxisome and mitochondrion share the same ancestor (Kuroiwa et al. 2008; Imoto et al. 2011a) [Fig. 2-25 Peroxisome (3)]. The first idea is based on the observations that peroxisomes are physically attached to the ER and peroxisome biogenesis factor (PEX) 3 and PEX19 localized to peroxisomes

from the ER in *Saccharomyces cerevisiae* (Hoepfner et al. 2005). However, physical attachment was also observed between mitochondria and ER (Kornmann et al. 2009; Yagisawa et al. 2013) and localization of PEX3 and PEX19 at the ER was not conserved in mammalian and land plant cells (Fang et al. 2004; Hunt & Trelease 2004; Hu et al. 2012). In *C. merolae*, *de novo* formation of peroxisome by budding from the ER membrane was not observed and a single peroxisome proliferates by binary fission throughout the cell cycle (Miyagishima et al. 1999b; Imoto et al. 2011a; Yagisawa et al. 2013). The second idea is based on a consideration of catalase activity on the detoxification of hydrogen peroxides and the peroxisomal matrix protein import system. The development of peroxidatic or catalatic system is essential for aerobic life (Dolin 1961), therefore, the type of peroxide respiration in peroxisomes may have been characteristic of primitive aerobes (De Duve 1966). Peroxisome matrix proteins were made in the cytosol and transferred posttranslationally into the matrix by a system that relies, like that of endosymbiont descendants (mitochondria and chloroplasts), on the recognition of specific targeting signal sequences (PTS) (Gould et al. 1988). PTSs were classified into PTS1 and PTS2 which are conserved in almost all eukaryotic cells, and conserved sequences of PTS1 was also encoded in *C. merolae* genome (Matsuzaki et al. 2004; Nozaki et al. 2007). However, as the peroxisome lacks DNA, this idea was weak to prove (Schrader and Yoon 2007). The third idea is based on the consideration of peroxisome proliferation. Peroxisomes are autonomous organelles that multiply by growth and division, like mitochondria and chloroplasts (Lazarow and Fujiki 1985; Miyagishima et al. 1999b; Imoto et al. 2011a). However, it has not been discussed about the division machinery of peroxisome.

To give the new insight on the origin of peroxisome, I discuss the origin of organelles in the view of their division machinery. The membrane-bounded organelle inheritance is classified into three units that the organelle partners accompanying the division: the cell-nuclear unit is composed of cell nuclear division accompanied by the division of ER and Golgi body (Yagisawa et al. 2012; 2013), the mitochondrial unit is composed of mitochondrial division accompanied by division of peroxisome and lysosomes, and the chloroplast unit is only chloroplast division (Miyagishima et al. 1999b; Yagisawa et al. 2007; Fujiwara et al. 2010; Imoto et al. 2011a). I consider that three partners seemed to evolve in order of the cell-nuclear unit, the mitochondrial unit and the chloroplast unit (Kuroiwa et al. 2008), each with respective partners. Mitochondria and chloroplast which are representative organelles in each partner originated by endosymbiosis after phagocytosis of α-proteobacteria and cyanobacteria, respectively (Margulis 1970; Gillham 1994; Cavalier-Smith 2000). This idea is supported by the data indicating that mitochondria are divided by electron dense MD machinery (Kuroiwa et al. 1982), while chloroplast are divided by electron dense PD machinery (Mita et al. 1986). The MD machinery consists of the matrix inner machinery, which includes the inner MD and filament temperature-sensitive mutant Z (FtsZ) rings including FtsZ1 which originated from bacterial cell division machinery, and the cytosolic outer machinery consist of filamentous structure with the dynamin family member Dnm1(Nishida et al. 2003; Yoshida et al. 2009). The PD machinery consists of the stromal inner machinery, which includes the inner PD and FtsZ rings including FtsZ2 which originated from bacterial cell division machinery, and the cytosolic outer machinery consist of the bundle of polyglucan with the dynamin family member Dnm2

(Miyagishima et al. 2003; Yoshida et al. 2010). In this study, I showed that peroxisomes were divided by the POD machinery consisted of DB ring and filamentous ring (Fig. 2-17). The DB ring was an amorphous string and included Dnm1 (Fig. 2-17). Dnm1 was also included in the MD machinery (Nishida et al. 2003; Yoshida et al. 2009), and was involved in both the fission of mitochondrion (Nishida et al. 2003) and the contraction and fission of peroxisome (Fig. 2-7, Fig. 2-22 and Fig. 2-23). The molecular genetic studies in animal, land plants and yeast suggested that Dnm1 ortholog proteins were involved in both mitochondrial and peroxisomal divisions (Bleazard et al. 1999; Koch et al. 2003; Fujimoto et al. 2009). While the cell nucleus unit and endomembrane organelles used dynamin DYN1 or VPS1 which are phylogenetically distinct from Dnm1 family members and chloroplast used Dnm2 which shares common ancestor with and transferred from cytokinesis dynamin (Miyagishima et al. 2009), the POD machinery contained Dnm1 and the same dynamin as the MD machinery. The filamentous ring was also major component of the POD machinery and contained fine filaments about 4 nm in diameter (Fig. 2-14). A bundle of fine filaments was also observed in the MD machinery by using electron microscopic analysis (Yoshida et al. 2009), implying a structural similarity between the filamentous ring of the POD machinery and MD machinery. Thus, these results suggest that POD machinery originates from the MD or pre-MD machinery. This supports the idea that the peroxisome originates from the common ancestor such as the premitochondrion, which originates from endosymbiotic α-proteobacterium [Fig. 2-25 Peroxisome (3)] (Kuroiwa et al. 2008; Imoto et al. 2013). This hypothesis is not conflicting with the function of peroxisomes and mitochondria. A metabolic link between peroxisomes and mitochondria is

found in fatty acid β-oxidation or glyoxylate cycles, and an exchange of metabolites between both organelles is required (Schrader and Yoon 2007). These metabolic interactions and communications show that mitochondria and peroxisomes dependent upon each other for their function and require coordinated inheritance regulations. Results in this study suggest the possibility that the POD machinery originates from the MD or pre-MD machinery and the host cell developed peroxisomes and mitochondria from the common ancestor distinct from the endomembrane system or chloroplasts.

Materials and Methods

Synchronization and isolation of dividing peroxisome fraction.

Cyanidioschyzon merolae 10D was used in this study (Toda et al. 1998). *C. merolae* was cultured in flasks, with shaking, under continuous light (40 W/m^2) at 42°C. For synchronization, cell cultures were subcultured to <1 × 107 cells/mL in a flat-bottom flask and subjected to a 12-h light/12-h dark cycle at 42°C using an automatic light/dark cycle CM incubator (Fujimoto Rika, Tokyo, Japan) (Suzuki et al. 1994). Synchronized cells were treated with a 1/2500 volume of 100 mM oryzalin stock solution dissolved in dimethyl sulphoxide (DMSO) after 8 h of the second light period. Cells were harvested at 12 h after the oryzalin treatment (late M phase). Cells were collected after centrifugation at 750 × g for 5 min, and incubated at 42°C in the dark for 40 min in isolation medium (20 mM Tris-HCl pH 7.6, 5 mM MgCl$_2$, 5 mM KCl, 5 mM EGTA) containing 180 mM sucrose, 40 mM oryzalin (hypotonic isolation medium), and 3 mg/mL Complete

EDTA-free protease inhibitor cocktail (Roche). Next, cells (2 × 108 cells/mL) were lysed in a French Pressure Cell (SLM-Aminco, Rochester, NY, USA) at 600 psi. After addition of 100 μg/mL DNase I and 0.5% w/v Triton X-100, the lysate was incubated for 1 h on ice, and then layered on a three-step Percoll gradient in 40-mL tubes (10 mL 60%, 10 mL 40%, and 4 mL 20% Percoll dissolved in isolation medium containing 300 mM sucrose [isotonic isolation medium]). After centrifugation at 23,000 × g for 50 min in a swinging-bucket rotor (P28S; Hitachi Koki, Tokyo, Japan), the fraction at the 40% Percoll interface was incubated in isotonic isolation medium containing 2% w/v Triton X-100 for 2 h on ice. And then, layered on a four-step Percoll gradient in 40-mL tubes (5 mL 40%, 5 mL 25%, 10 mL 10% and 2 mL 0% Percoll dissolved in isotonic isolation medium). After centrifugation at 18,000 × g for 60 min in a swinging-bucket rotor, the fraction at the 25% Percoll interface was dissolved in sucrose-free isotonic isolation medium containing 500 mM n-octyl-β-D-glucopyranoside [OG] for 30 min on ice. Then, layered on a 0.5 mL 10 % Percoll dissolved in sucrose-free isotonic isolation medium. After centrifugation at 8,000 × g for 30 min, dividing-peroxisome fraction was located at bottom pellet. This fraction was washed once with sucrose-free isotonic isolation medium by centrifugation at 700 × g for 20 min. The isolated dividing peroxisomal fraction was resuspended in sucrose-free isotonic isolation medium at a concentration of 1 mg total protein/mL.

Proteomic analysis of dividing-peroxisome fraction

Samples were analyzed by a peptide mass fingerprinting (PMF) search using a MALDI-TOF mass spectrometer AXIMA-TOF2 (Shimadzu, Kyoto,

Japan) in reflectron mode. Database searches were performed using the software program MASCOT v2.2.01 (Matrix Science, MA, USA) running on the local server against the *C. merolae* genome database (including 5014 sequences), based on the FASTA file distributed by the Cyanidioschyzon merolae Genome Project (http://merolae.biol.s.u-tokyo.ac.jp/) (Matsuzaki et al. 2004; Nozaki et al. 2007). The permissible value of missed cleavages was set at one. Identified proteins with a MASCOT score greater than 50 are shown in Table S1.

Immunological analysis

For immunoblotting, 20 μg total protein extract from *C. merolae* was separated on 12.5% sodium dodecyl sulphate–polyacrylamide gels, and then transferred onto polyvinylidene difluoride membranes. After blocking with 5% skim milk in Triton X-100 Tris-buffered saline (TTBS), the membranes were incubated with primary antibodies; anti-Dnm1 rabbit antibody (Nishida et al. 2003) (1:1000 dilution), anti-catalase rat antibody (Ohnuma et al. 2009) (1:2000 dilution), anti-porin guinea pig antibody (Fujiwara et al. 2009b) (1:1000 dilution), anti-Mda1 mouse antibody (Nishida et al. 2007) (1:1000 dilution), and anti-PDR1 rat antibody (Yoshida et al. 2010) (1:500 dilution) in TTBS. Alkaline phosphatase-conjugated goat anti-rabbit, rat, mouse, or guinea pig IgG was used at a dilution of 1/1000 as the secondary antibody. Signals were detected using an alkaline phosphatase (AP) conjugate substrate kit (Bio-Rad, Hercules, CA, USA). For immunofluorescence microscopy, cells were fixed and blocked as described previously with minor modifications (Nishida et al. 2004). As primary antibodies, I used anti-Dnm1 rabbit

antibody (1:200 dilution), anti-catalase rat antibody (1:500 dilution), anti-porin guinea pig antibody (1:500 dilution), anti-Mda1 mouse antibody (1:200 dilution) anti-FtsZ1 mouse antibody (Takahara et al. 2000) (1:500 dilution) and anti-Dnm2 rabbit antibody (Miyagishima et al. 2003) in PBS. As secondary antibodies, I used Alexa Fluor 488 or Alexa Fluor 555 goat anti-rabbit, anti-mouse, or anti-rat IgG (1:1000 dilution). Images were captured using a fluorescence microscope BX51 (Olympus, Tokyo, Japan). Isolated POD machineries were left unfixed in PBS. Primary antibody reactions were performed for 1 h at 37°C with rabbit anti-Dnm1 diluted 1:1000 in PBS. For the secondary antibody reactions, the primary antibodies were detected with Alexa Fluor 488 goat anti-rabbit IgG for 1 h at 4°C. For microfluorometry, the intensity of fluorescence was quantified using a VIMPCS as described previously with minor modifications (Imoto et al. 2010). The relative fluorescence intensity of particles and dynamin rings of dynamin-like protein Dnm1 were calculated at each sampling time. The signal intensity ratio of Dnm1 was calculated based on signal intensities of the whole rings.

Isolation of POD machinery

The isolated dividing-peroxisome fraction was dissolved in peroxisome membrane dissolution buffer (PBS containing 3 mM sodium lauryl sulphate, 10 mM urea) and incubated at 4°C for 2 min. Isolation of the PD-ring was performed described as previously (Yoshida et al. 2006).

Negative staining and immunoelectron microscopy

The fraction containing POD machineries with the peroxisome membrane, which was insoluble after 0.5% triton X-100 treatment, was left unfixed. Primary antibody reactions were performed for 1 h at 4°C with anti-Dnm1/DRP3 (diluted 1:10 in PBS), followed by a secondary reaction for 1 hour at 37°C with goat anti-rabbit IgG conjugated with 15-nm colloidal gold (diluted 1:10; British BioCell International, Cardiff, UK). For double labelling, anti-dynamin reacted samples were incubated with anti-catalase (diluted 1:200 in PBS), followed by a secondary reaction with goat anti-rat IgG conjugated with 10-nm colloidal gold (diluted 1:10; British BioCell International). Then, samples were incubated in PBS containing 3 mM sodium lauryl sulphate and 10 mM urea for 15 min on ice, and the lysates were negatively stained with 0.5% phosphotungstic acid (pH 7.0). Samples were examined using an electron microscope (model JEM-1200; JEOL, Tokyo, Japan) (Yoshida et al. 2010). The labeling density of catalase and Dnm1 at each site was quantified as described previously (Nishida et al. 2003) by using an Image-J.

Plasmid construction and transformation

The plasmids pMtGFP and pMtGFP-Dnm1AS were used in the antisense suppression assay of Dnm1. To construct pMtGFP, the promoter region (780 bp) and 5' portion (220 bp) of the EF-Tu gene (CMS502C), which includes a mitochondrial transit peptide, was amplified from *C. merolae* genomic DNA with the primers 5'- cgcGGATCCtgaagtggcgagatcgtcgc-3' (BamHI site capitalized) and 5'- gcgcAGATCTgcgtttgcttgcactcgcct-3' (BglII site capitalized) in 25 cycles (98°C for 10 s, 60°C for 30 s, and 72°C for 1 min) using PrimeSTAR® HS DNA polymerase (TaKaRa Bio, Otsu,

Japan). The amplified fragment (1000 bp) was digested with BamHI and BglII (TaKaRa) and inserted into the BamHI site of pTH2PL35 to make pMtGFP. To create a CmDnm1 antisense suppression construct regulated by the Dnm1 promoter, the Dnm1 promoter-Dnm1 antisense fused DNA fragment was amplified by overlap extension PCR. To obtain the antisense strand of the Dnm1 ORF adjacent to the promoter region, the promoter region and the antisense strand of the Dnm1 ORF were amplified individually. Using the oligonucleotide primers Dnm1_PromF_HindIII (5′-gcgcAAGCTTttcctccattctttcaaag-3′ (HindIII site capitalized)) and Dnm1prom_R (5′-ttcacgtcaaagaggagattgaagcctgtcgcgttcgccc-3′; overlapped sequence underlined) and *C. merolae* DNA as a template, the promoter region of the Dnm1 gene (1,064 bp) was amplified. PCR was carried out for 30 cycles (98°C for 10 s, 55°C for 5 s, and 68°C for 1 min) with PrimeSTAR® HS DNA polymerase (TaKaRa). Similarly, the antisense strand of the Dnm1 ORF (2,304 bp) was amplified using the oligonucleotide primers Dnm1ASORF_F (5′-gggcgaacgcgacaggcttcaatctcctctttgacgtgaa-3′; overlapped sequence underlined) and Dnm1ASORF_R (5′-catTCTAGAatggagcgcctaatacctatc-3′; XbaI site capitalized). Amplified fragments of the Dnm1 promoter region and the antisense strand of the Dnm1 ORF were separated by electrophoresis and purified using the QIAquick Gel Extraction kit (QIAGEN, Hilden, Germany). PCR (98°C for 10 s, 60°C for 5 s, and 68°C for 3.5 min) was performed with these fragments without template for 10 cycles to make a fused DNA fragment (3,387 bp). Then, using the fused fragment as a template, PCR was carried out with the primers Dnm1_PromF_HindIII and Dnm1ASORF_R for 20 cycles (98°C for 10 s, 55°C for 5 s, and 68°C for 3.5 min) to amplify a

DNA fragment of the antisense strand of the Dnm1 ORF adjacent to the promoter region. The amplified fragment was digested with HindIII and XbaI and substituted for the HindIII–XbaI fragment of pMtGFP to make pMtGFP-Dnm1AS. The resultant plasmids, pMtGFP (control) and pMtGFP-Dnm1AS (for antisense suppression of Dnm1), contained an EF-Tu transit peptide-sGFP sequence driven by the EF-Tu promoter; therefore, transformed cells could be detected by green fluorescence under a fluorescence microscope. Transformation of *C. merolae* cells was performed as described previously (Ohnuma et al. 2009) with minor modifications. Cells were collected 24 h after introduction of DNA, transferred to new MA2 medium, and then incubated for another 24 h.

Table 2-1. Proteomic analysis of isolated peroxisomal fraction at 20h in back ground and Oryzalin-treated cells.

Background

*	Locus	Annotation	expect
1	CMV157	[pt] phycobilisome linker polypeptide	7.90E-13
2	CMQ054C	hypothetical protein, conserved	0.00032
	CMA044C	cryptochrome DASH	0.011
3	CMH197C	mitochondrial F-type ATPase F1 subunit beta, precursor	0.00037
	CMR087C	hypothetical protein, conserved	0.028
4	CMI050C	catalase †	0.0015
5	CMV196C	ATP synthase CF1 beta chain	4e-006
6	N.D.		
7	CMD067C	probable prohibitin protein	0.0013
	CML334C	hypothetical protein, conserved	0.0046
	CMM221C	hypothetical protein	0.006
8	CMV051C	phycobilisome rod-core linker polypeptide	1.6e-006
9	CMV155C	cytochrome f	0.03
10	N.D.		

Oryzalin treated cells

*	Locus	Annotation	expect
1	CME019C	dynamin-related protein involved in mitochondrial division CmDnm1/DRP3	6.60E-04
2	CMI157C	ATP-dependent zinc protease	0.0023
3	CMD101C	unknown GTP-binding protein	2.1E-005
	CMT273C	Type II DNA topoisomerase VI subunit B	0.0053
	CMH197C	mitochondrial F-type ATPase F1 subunit beta, precursor	0.0085
	CMQ241C	probable plastid-specific ribosomal protein PSRP-1 precursor	0.032
4	CME141C	similar to GTP-binding protein	0.035
	CMT322C	chaperonin containing TCP1, subunit 2 (beta)	0.02
5	CMQ295C	cell division protein FtsH	0.0044
	CMS291C	similar to FKBP-type peptidyl-prolyl cis-trans isomerase Mip	0.0096
	CME103C	hypothetical protein, conserved	0.037
	CML258C	hypothetical protein	0.051
6	CMI050C	Catalase †	2.00E-07
7	CMO274C	V-type ATPase V0 subunit d	0.042

8	CMS429C	serine-glyoxylate aminotransferase †	7.40E-05
	CMT344C	hypothetical protein, conserved	0.0047
9	CMD105C	similar to peroxisomal membrane protein PEX2 †	0.011
10	CMD067C	probable prohibitin protein	0.0013
	CML334C	hypothetical protein, conserved	0.0035
	CMS224C	hypothetical protein, conserved	0.0045
11	CML063C	hypothetical protein	1.30E-06
	CMV051C	phycobilisome rod-core linker polypeptide	1.60E-04
12	CMI290C	manganese-stabilzing protein precursor	0.00046
	CMV155C	cytochrome f	0.0024
13	CMN155C	probable beta-alanine synthase, closer	0.013

Mascot scores higher than 50 are shown. Odd numbers are shown in bold.

ND, not detected.

*The numbers coincide with the bands in Fig. 2-3, respectively.

† Known peroxisomal proteins.

Table 2-2. Quantitative calculation of immunolabeling density at each site against catalase and Dnm1

Site *	Labeling Density (mm^{-2}) [#]	
	Catalase (10nm)	Dnm1 (15nm)
Membrane	433.9 ± 62.1	15.0 ± 14.1
POD ring	44.2 ± 17.3	304.0 ± 45.9

* Examined sites are listed as Membrane (partially dissolved peroxisome membrane, excluding POD ring), POD ring.
[#] Values are indicated as means ± standard deviation of the number of gold particles. n=10

Table 2-3. Features of peroxisome-dividing (POD) machineries and comparison to mitochondrion-dividing (MD) and plastid-dividing (PD) machineries

Organelles	Peroxisome	Mitochondrion	Chloroplast
Membrane	Single	Double	Double
DNA	-	+	+
Division machinery	POD	MD	PD
Diameter of division site (sectioned) (nm)	500 (250)	750 (730*)	1000 (1270*)
Isolated machinery	POD	MD	PD
Structure			
Shape	Ring	Irregular	Ring‡
Diameter (nm)	50 – 600	150 – 1200 †	150 – 1300‡
Width (nm)	25 – 30	N. D.	20 – 130
Supertwist	-	N. D.	+
Composition			
Filament (nm) (component)	4 ~ 5 (N. D.)	N. D.	5~7(polyglucan)
Dynamin homolog	Dnm1/DRP3	Dnm1/DRP3†	Dnm2/DRP5‡
FtsZ homolog	-	FtsZ1†	FtsZ2‡
Mdv1 homolog	N. D.	Mda1†	N. D.
Glycosyltransferase	-	N. D.	PDR1‡

N.D., not detected.

*The diameter of the MD ring was calculated by the circumference from Miyagishima et al. (1999a).

†Data for the features of the isolated MD ring is from Yoshida et al. (2009)

‡Data for the features of the isolated PD ring is from Yoshida et al. (2010)
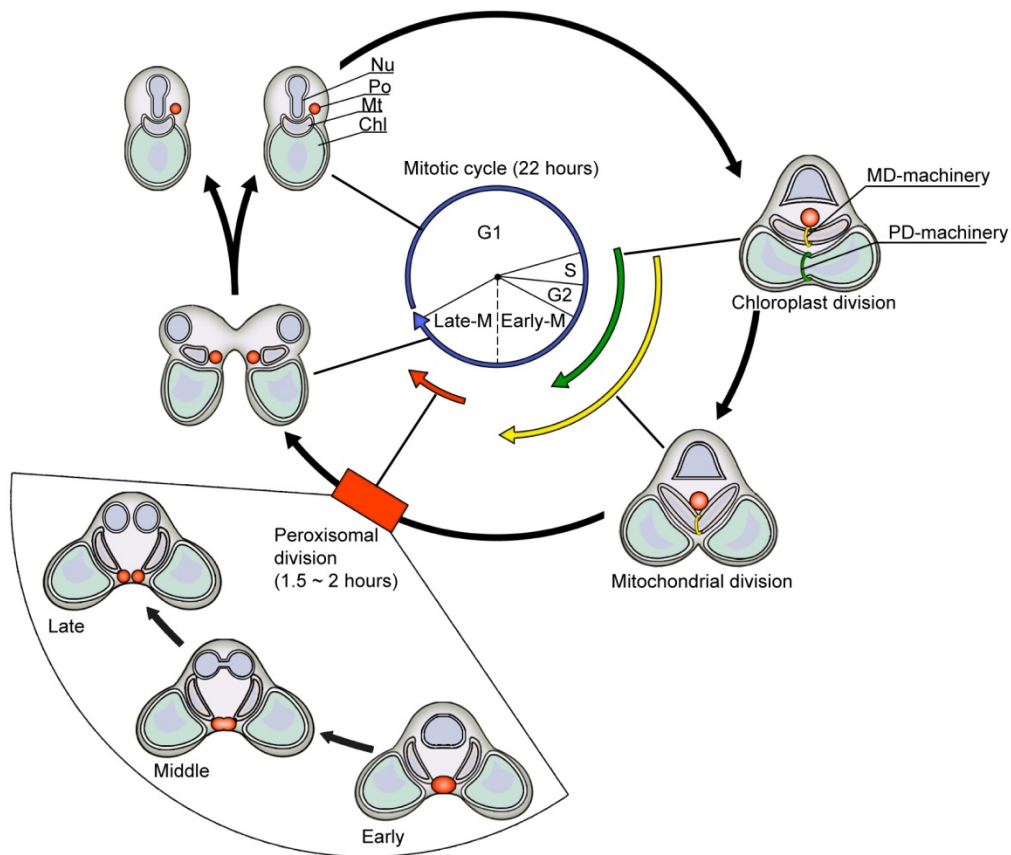
Fig. 2-1. Schematic representation of the timing of chloroplast, mitochondrial, and peroxisomal divisions during the cell cycle.

The duration of the mitotic cycle of *C. merolae* is 19 ~22 h. The chloroplast, mitochondrion, cell nucleus, and peroxisome divide in that order. Chloroplast (green arrow) and mitochondrial (yellow arrow) divisions occur during S–G2 phase and early M phase (prophase). Peroxisomal division (1.5–2 h) (red arrow) occurs during late M phase (anaphase) after mitochondrial division. Oval-shaped peroxisomes become dumbbell-shaped from the early to middle periods of the division and finally divide into two daughter peroxisomes by binary fission. Chl, chloroplast; Mt, mitochondrion; Nu, cell nucleus; Po, peroxisome.

61
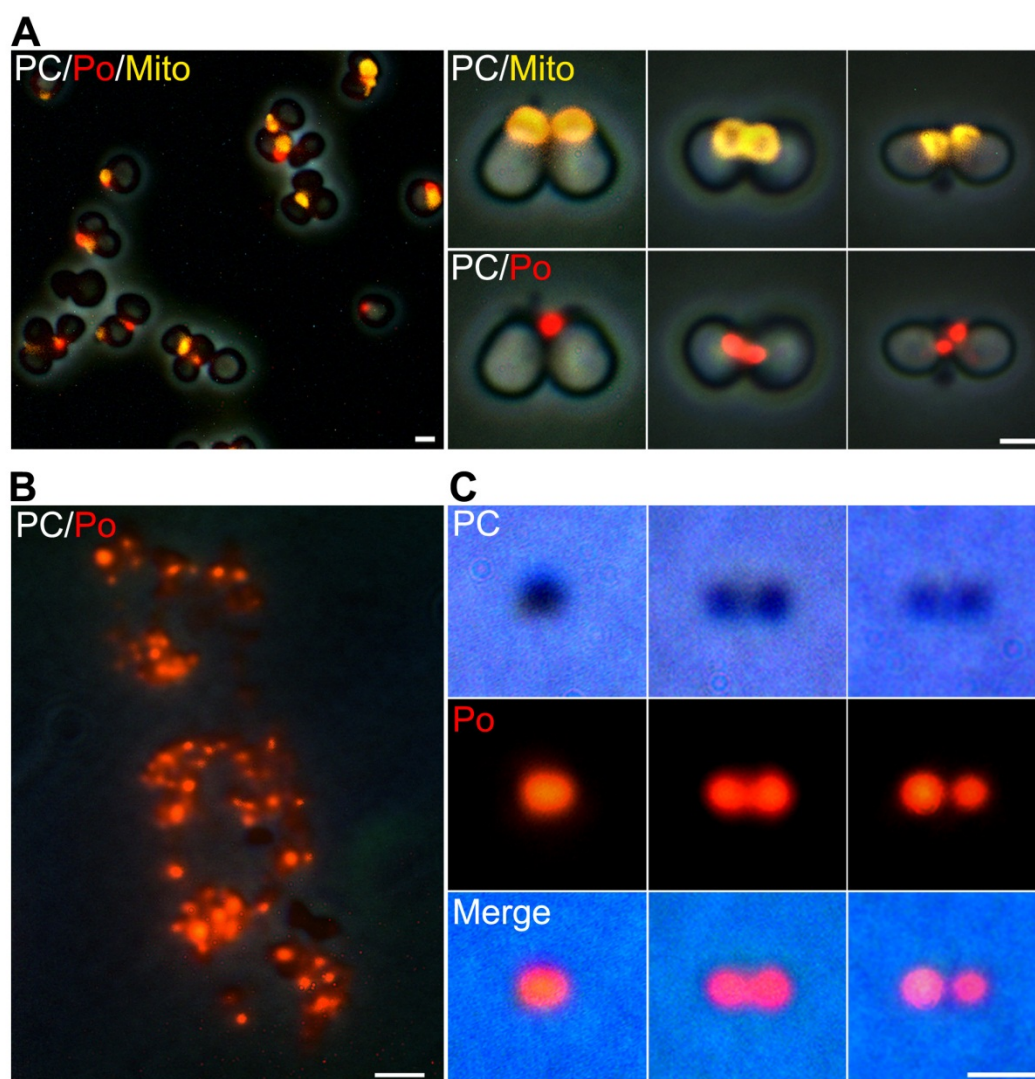
Fig. 2-2. Isolation of dividing peroxisomes.

(A) Phase-contrast and immunofluorescence images of isolated organelle complexes contain divided mitochondria (Mito, yellow, anti-porin), divided chloroplast and dividing or divided peroxisomes (Po, red, anti-catalase). Scale bars: 1 μm. (B) Phase-contrast (PC) and immunofluorescence images of peroxisomes (red, anti-catalase) in the dividing peroxisomal fraction. (C) Enlarged images of a dividing peroxisome (Po, red, anti-catalase) in the dividing-peroxisomal fraction. Scale bars: 1 μm.
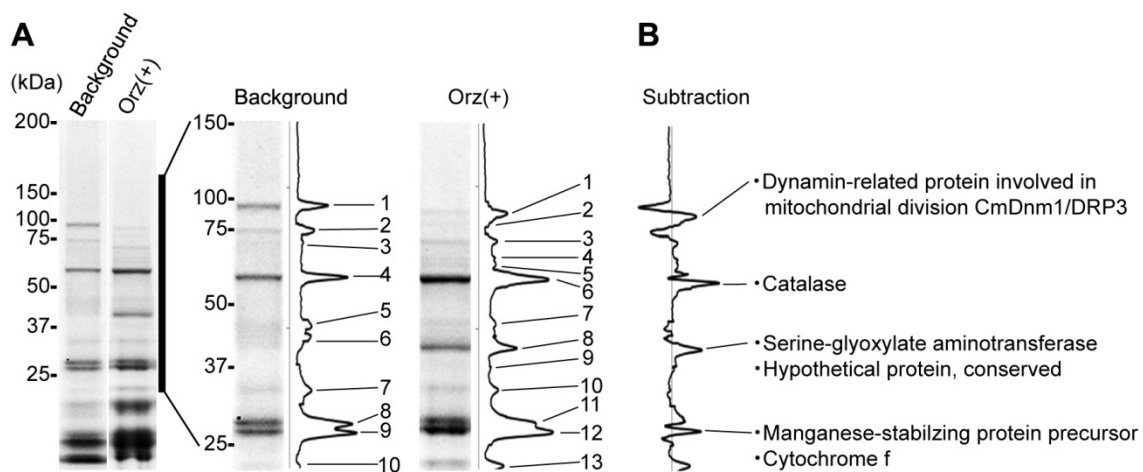
Fig. 2-3. Proteomic analysis of dividing peroxisome fraction.

(A) Proteins in the isolated peroxisomal fractions from background (Orz-) and oryzalin-treated cells (Orz+) at 20 h. The gel image on the right is an enlarged image of the left gel image (bar). Ten (background) and 13 (oryzalin-treated cells) bands are identified by MALDI-TOF mass spectrometry. The numbers of identified proteins are described in Table 2-1. (B) Major subtracting bands from those of the peroxisomal fractions in control and oryzalin-treated cells. The three major peaks were identified as CmDnm1/DRP3 (Dnm1), catalase, and serine-glyoxylate aminotransferase. Catalase and serine-glyoxylate aminotransferase are known to be peroxisomal proteins.
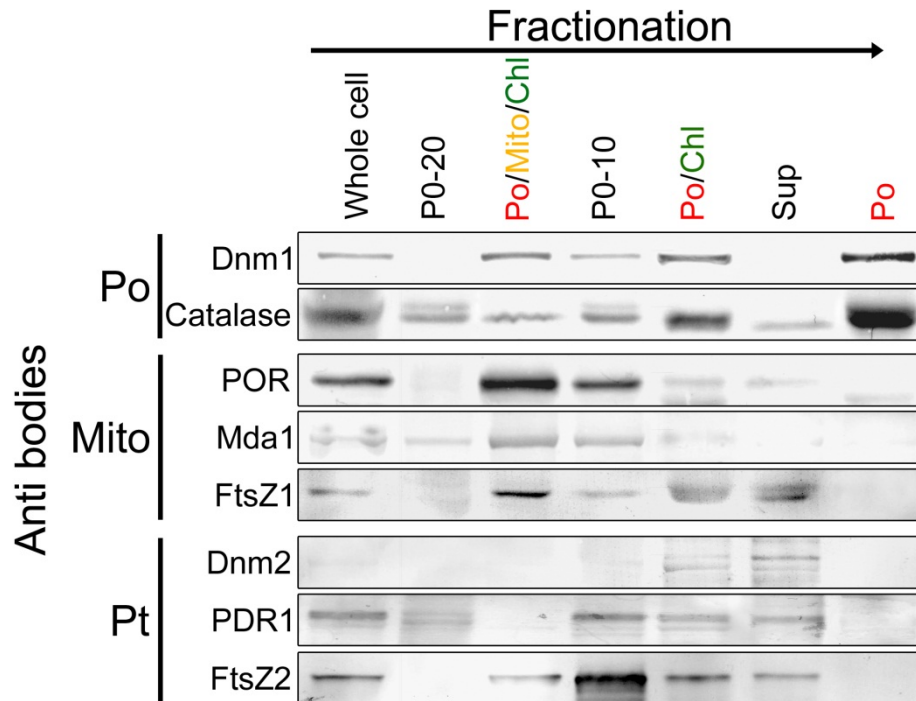
Fig. 2-4. Immunoblot analyses throughout the fractionation processes.

Dnm1, catalase, porin, mitochondria division protein (Mda1), FtsZ1, Dnm2, PDR1 and FtsZ2 were examined. Dnm1 and catalase were concentrated in peroxisomal fraction. P0-20, 0-20% Percoll gradient layer appeared after the centrifugation of cells lysed in French pressure; Po/Mito/Chl, organelle complex fraction appeared at the 40% Percoll interface. P0-10, 0-10% Percoll gradient layer appeared after the centrifugation of detergent treated Po/Mito/Chl fraction; Po/Chl, dividing or divided peroxisomes with partially lysed chloroplasts fractions; Sup, supernatant appeared after the centrifugation of detergent and hypotonic treated Po/Chl fraction; Po, dividing or divided peroxisomal fraction.

64
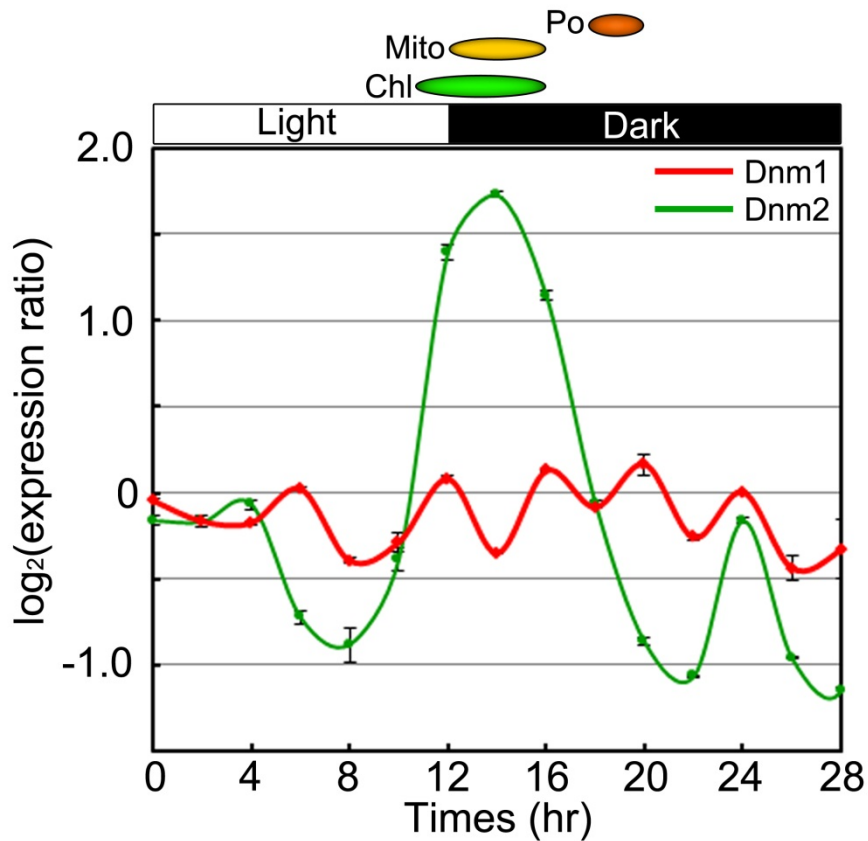
Fig. 2-5. Microarray analysis of dynamins throughout cell cycle.

Microarray analysis of synchronized *C. merolae* (Fujiwara et al. 2009) during the cell cycle showed that Dnm1 transcribed continuously throughout cell cycle and Dnm2 transcribed during chloroplast division. Chl, chloroplast division period; Mito, mitochondrial division period; Po, peroxisomal division period.
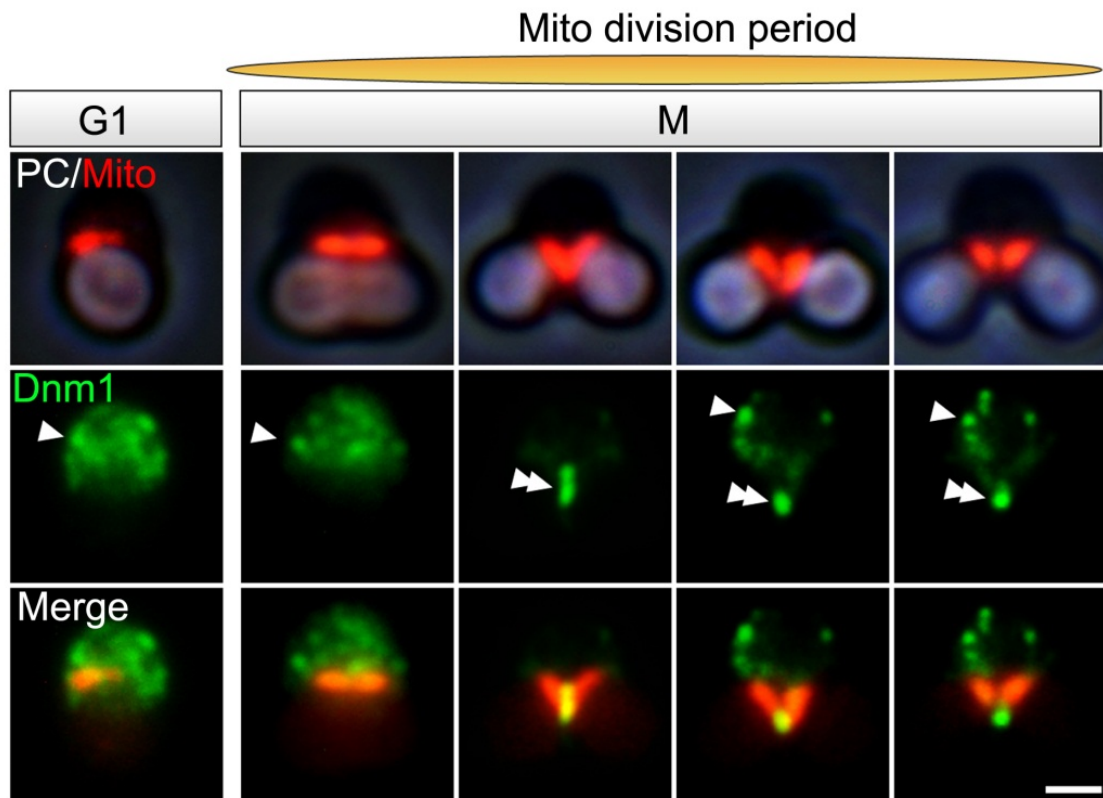
Fig. 2-6. Dnm1 localizations during G1 phase and the mitochondrial division period (early M phase).

 Phase contrast immunofluorescence microscopic images of Dnm1 (anti-Dnm1) and mitochondria (Mito, anti-EF-Tu). Dnm1 localized in cytosol as dynamin patches (arrowhead) and recruited to the mitochondrial division site (double arrowhead) during early M phase.

Scale bar: 1 μm.
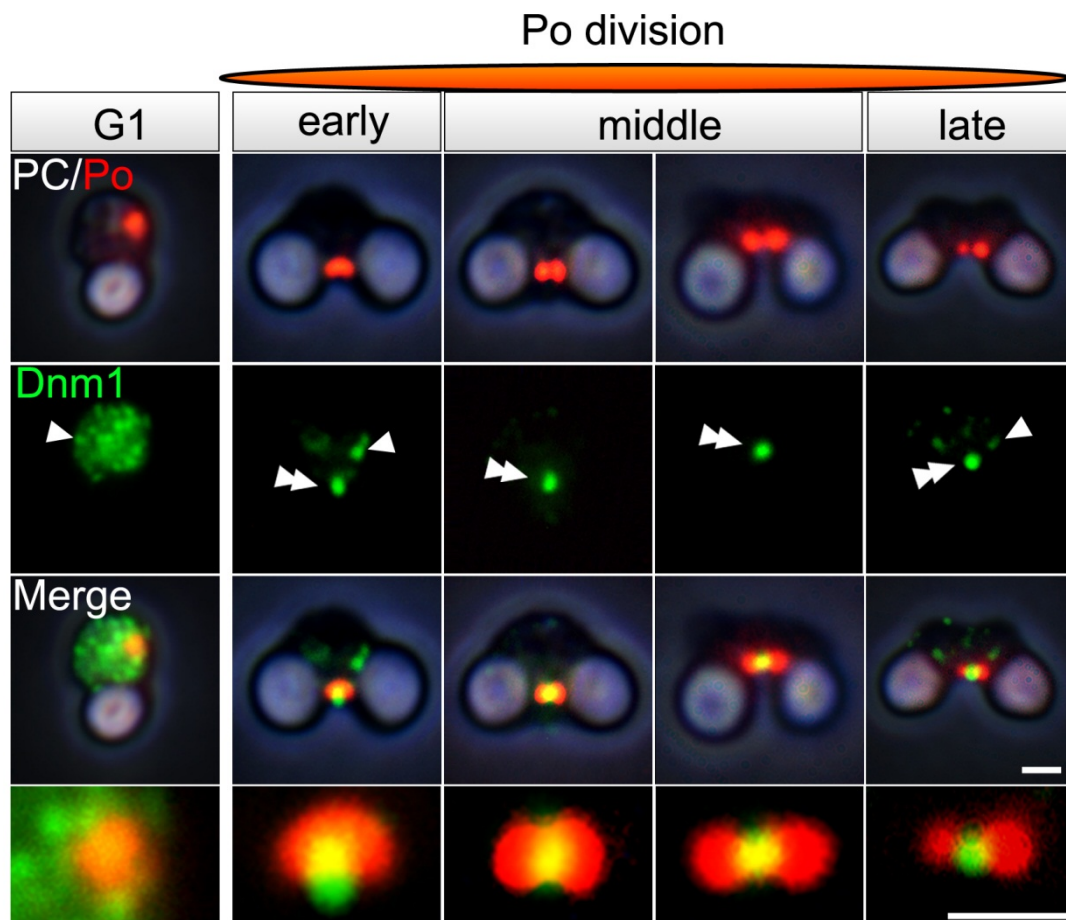
Fig. 2-7. Dnm1 localizations during G1 phase and the peroxisomal division period (late M phase).

Phase contrast immunofluorescence microscopic images of Dnm1 (anti-Dnm1), peroxisome (Po, anti-catalase) and enlarged merged images. Dnm1 localized in cytosol as dynamin patches (arrowhead) and recruited to the peroxisomal division site (double arrowhead) during late M phase. Scale bar: 1 μm.
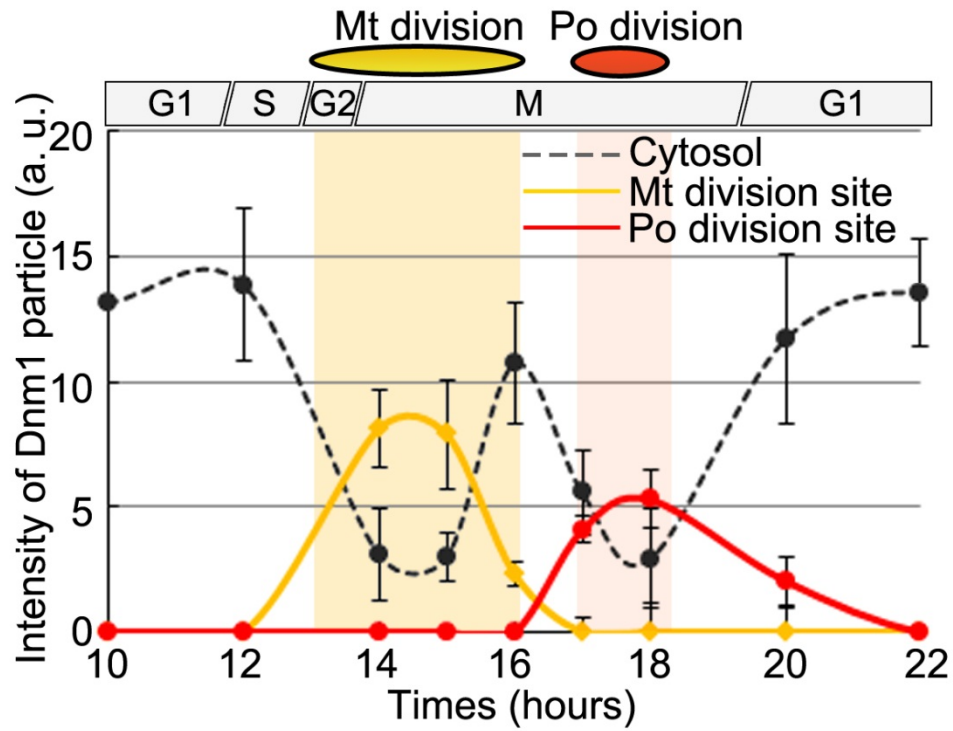
Fig. 2-8. Microfluorometry analysis of Dnm1 throughout cell cycle.

  Dynamic change of Dnm1 signals between the cytosol (dotted line) and division site of mitochondrion or peroxisome (solid line). n=3, 50>cells.
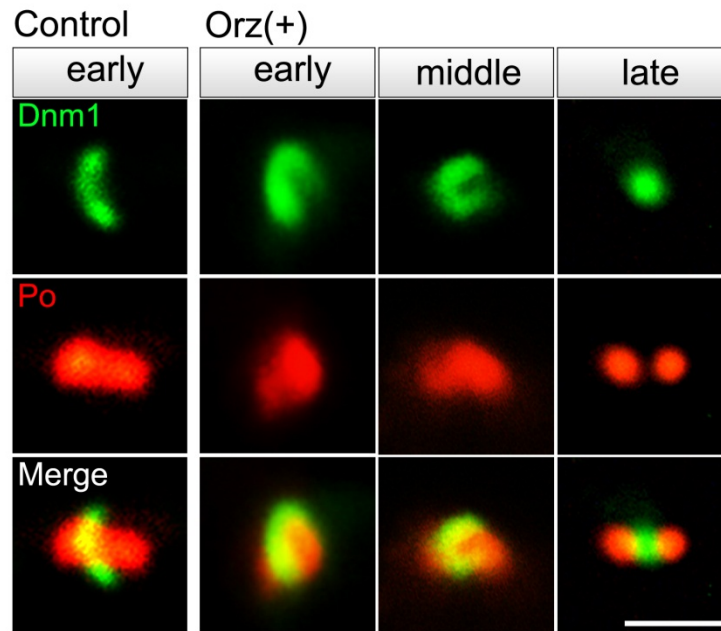
Fig. 2-9. Dynamin ring-like structures at the peroxisomal division site.
Immunofluorescence images of the dynamin ring-like structures (green, anti-Dnm1) encircling dividing peroxisomes (red, Po, anti-catalase) in slightly squashed control (Orz-) and oryzalin-treated cells (Orz+). Scale bar: 1 μm.
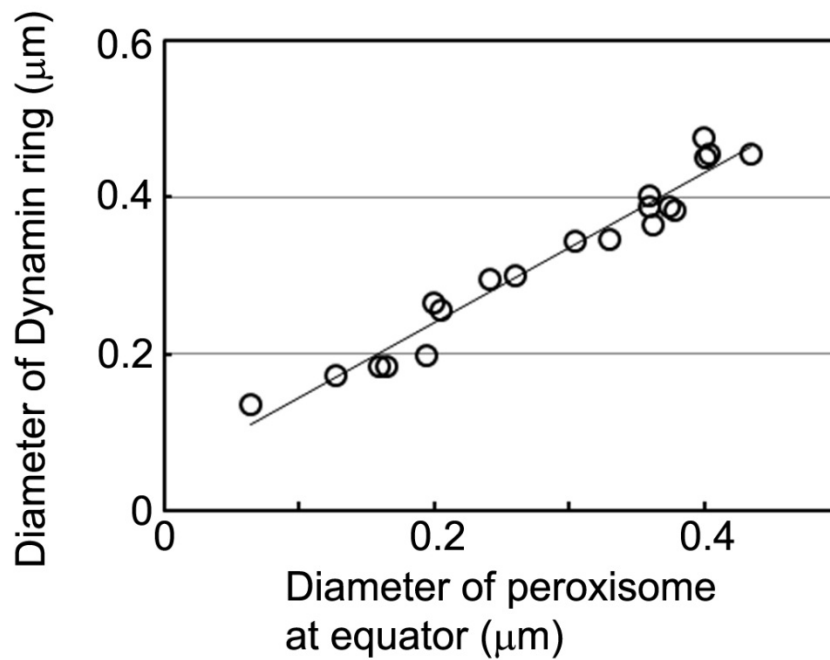
Fig. 2-10. Diameter plots of dynamin rings against diameter of peroxisomal division plane.

  The diameter of the dynamin rings immunostained by using anti-Dnm1 antibody was plotted against the diameter of the division site of peroxisomes immunostained by using anti-catalase antibodies. The diameter of the dynamin ring decreases as the diameter of the division site decreases during the peroxisome division process. n=20.
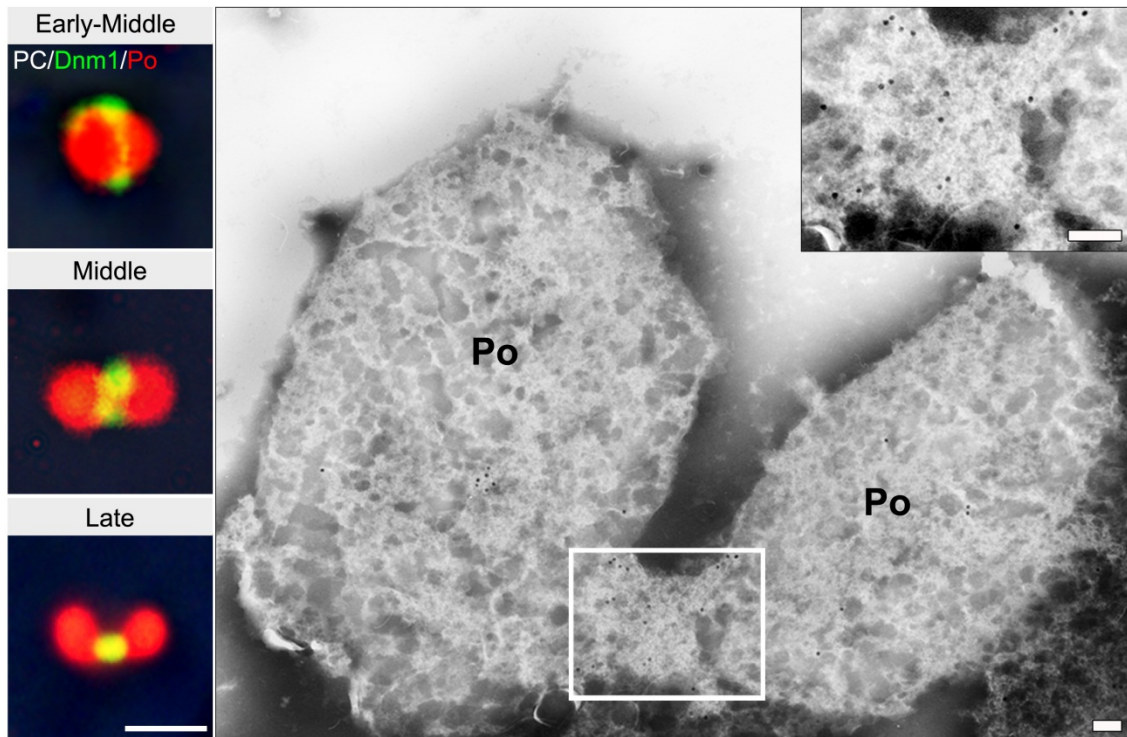
Fig. 2-11. Dnm1 localizations on isolated dividing peroxisomes.

 Phase contrast immunofluorescence images showing Dnm1 (anti-Dnm1) localized at the division plane of isolated peroxisomes (Po, anti-catalase). Immuno-EM image of isolated dividing peroxisome showed that 15 nm Dnm1-bound immunogold particles were visible on bridges between the daughter peroxisomes. Scale Bar: 1 μm (immunofluorescence microscopic images), 100 nm (immunoelectron microscopic images).
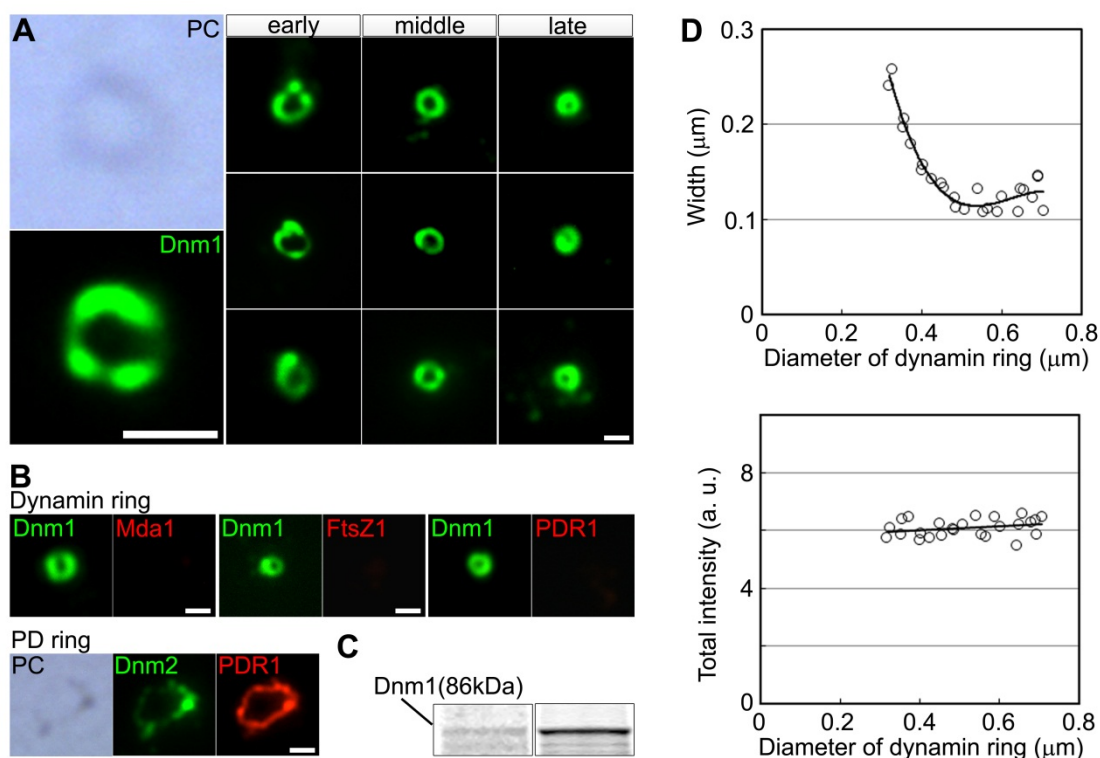
Fig. 2-12. Isolation of dynamin rings.

(A) Phase-contrast and immunofluorescence images of closed dynamin rings (anti-Dnm1) isolated from peroxisomes at various stages of division. (B) Immunofluorescence images of isolated dynamin rings from dividing peroxisomal fraction showing Dnm1 and Mda1, FtsZ1, or PDR1. Images of isolated PD ring showing Dnm2 and PDR1 as a control. (C) SDS/PAGE of the dividing-peroxisome fraction (Left) and isolated dynamin ring fraction (Right). (D) Width, and total fluorescence intensity of the Dnm1 signals relative to the diameter of the dynamin ring. Scale bars: 500 nm.
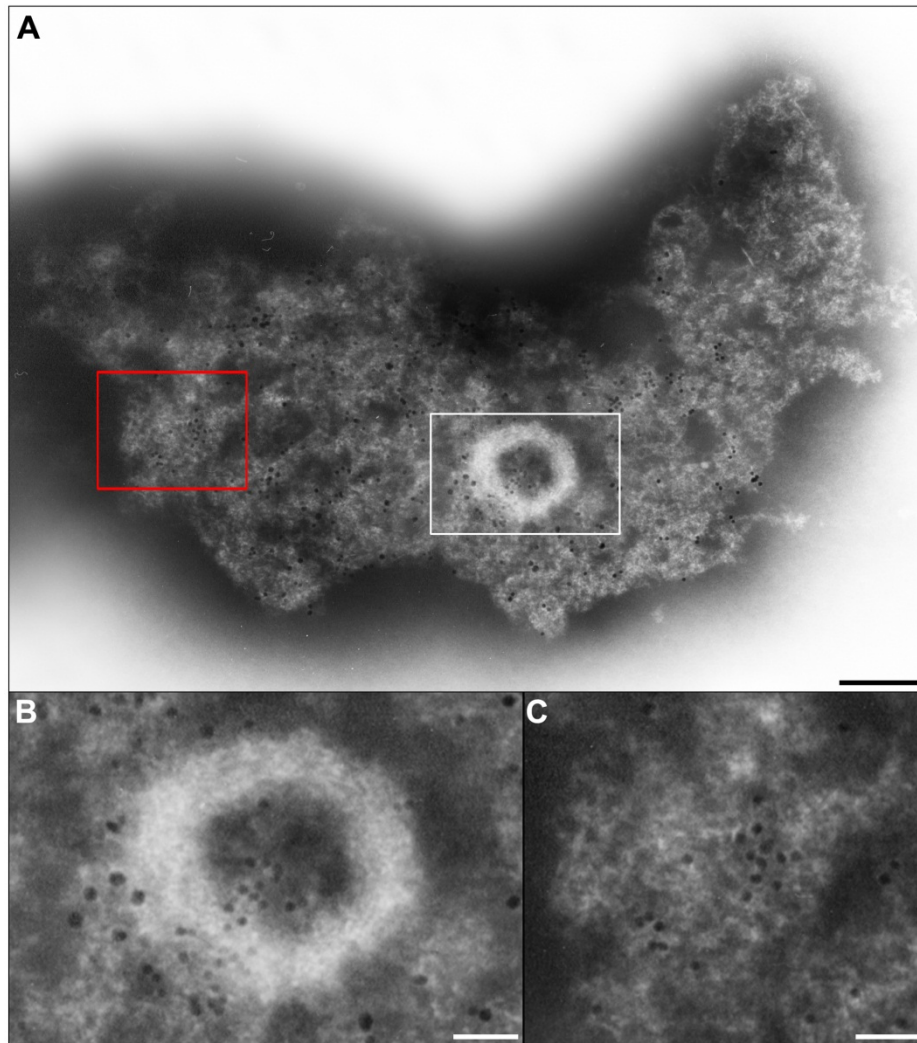
Fig. 2-13. Identification of skeletal filament of dynamin ring.

(A) Dnm1 is localized on the periphery of the skeletal filamentous ring, and catalase is localized on the membrane. (B) Enlarged micrograph of white box area in A. (C) Enlarged micrograph of the red boxed area in A showing partially dissolved peroxisome membrane by detergent treatment for 30 sec labeled with catalase. Large immunogold particles (15 nm), Dnm1; small immunogold particles (10 nm), catalase. Scale bars: 200 nm (A); 50 nm (B and C).
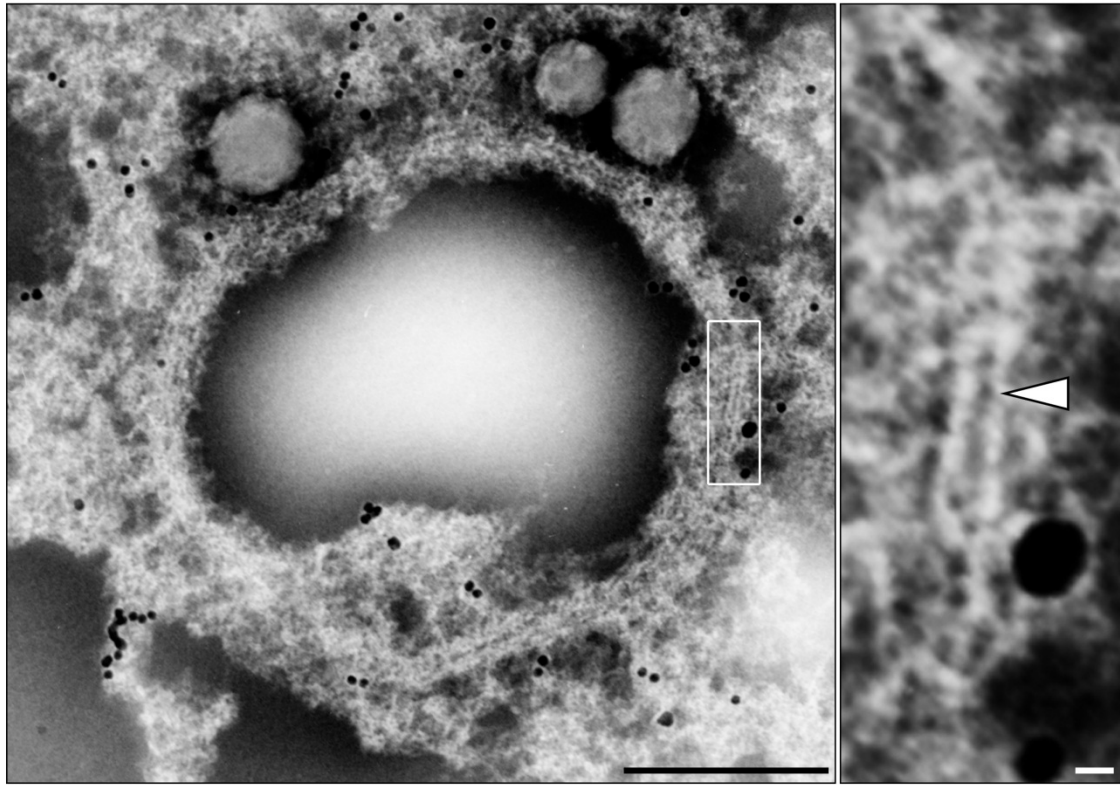
Fig. 2-14. Dynamin ring contains fine filament.

Immunoelectron microscopic image showed that skeletal filament contains fine filaments of about 4 nm in diameter (white arrow head). Immunogold particles (15 nm), Dnm1. Scale Bars: 200 nm (left panel); 10 nm (right panel, enlarged image).
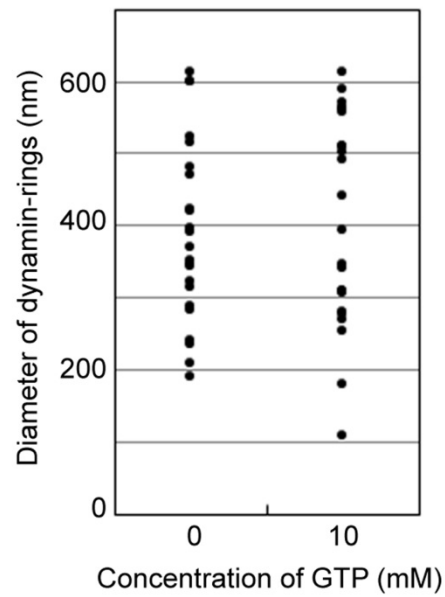
Fig. 2-15. **Effect of GTP on isolated dynamin rings.**

Comparison of the diameter of isolated dynamin rings before and after addition of 10 mM GTP (n = 25). A conformational change of the isolated dynamin ring is not induced by GTP addition.
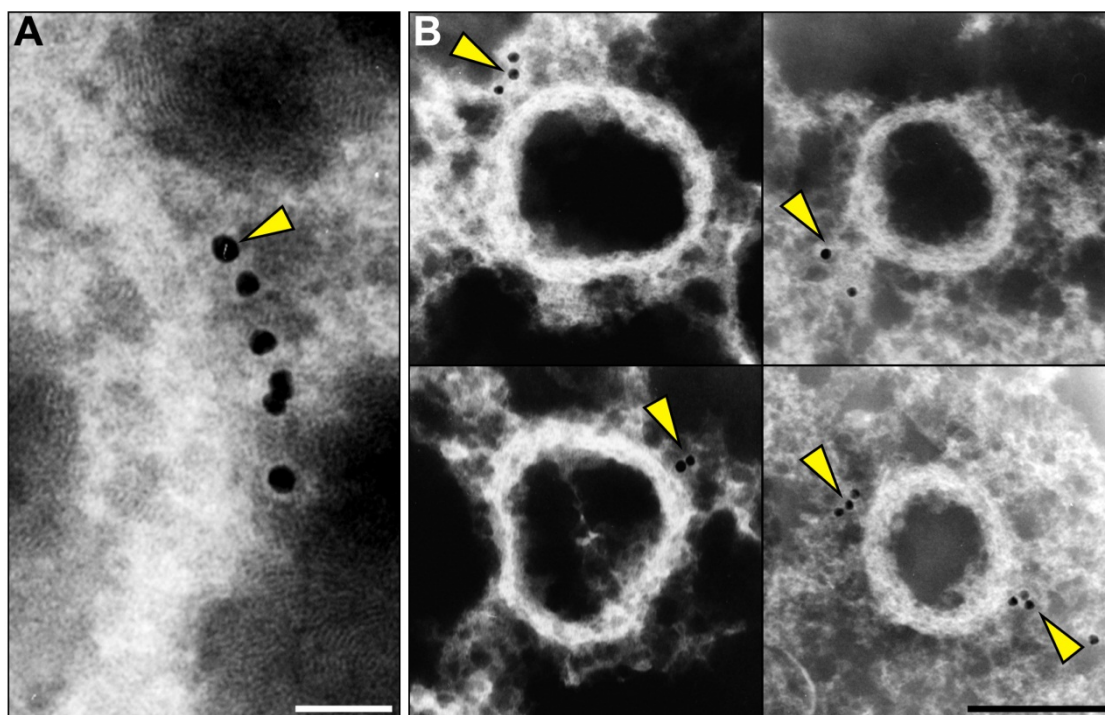
Fig. 2-16. Dnm1 localized at distances of about 10–20 nm along the skeletal filament.

(A) Dnm1-bound immunogold particles (yellow arrow head) arranged at a constant distance along the skeletal filamentous ring. (B) A few Dnm1 signals (yellow arrow heads) remain around the filamentous rings even after detergent treatment for 5 min. Scale bars: 50 nm (A); 200 nm (B).
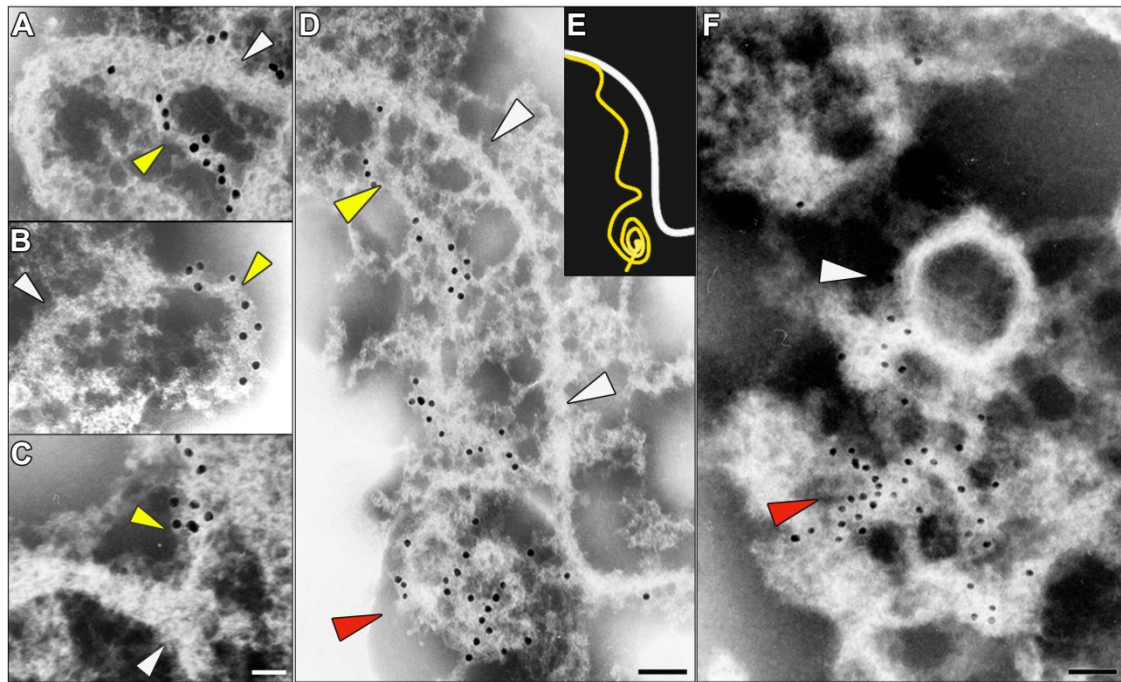
Fig. 2-17. Immuno-EM images and schematic representation showing the separation of the filamentous ring and the DB ring.

 (A–C) The DB rings (yellow arrowheads) are peeled off from the filamentous ring (white arrowheads) in parts of the POD machinery after the detergent treatment for 10 min. (D) The dynamin-based ring separated from the filamentous ring (white arrowheads) shows a string (yellow arrow head) and a part of the ring forms a clump (red arrowhead). (E) The schematic representation shows the dynamin-based ring (yellow line) and the filamentous ring (white line). (F) The DB ring separates from the filamentous ring (white arrowhead). Immunogold particles (15 nm), Dnm1. Scale bars: 50 nm (A-C); 100 nm (D and F).
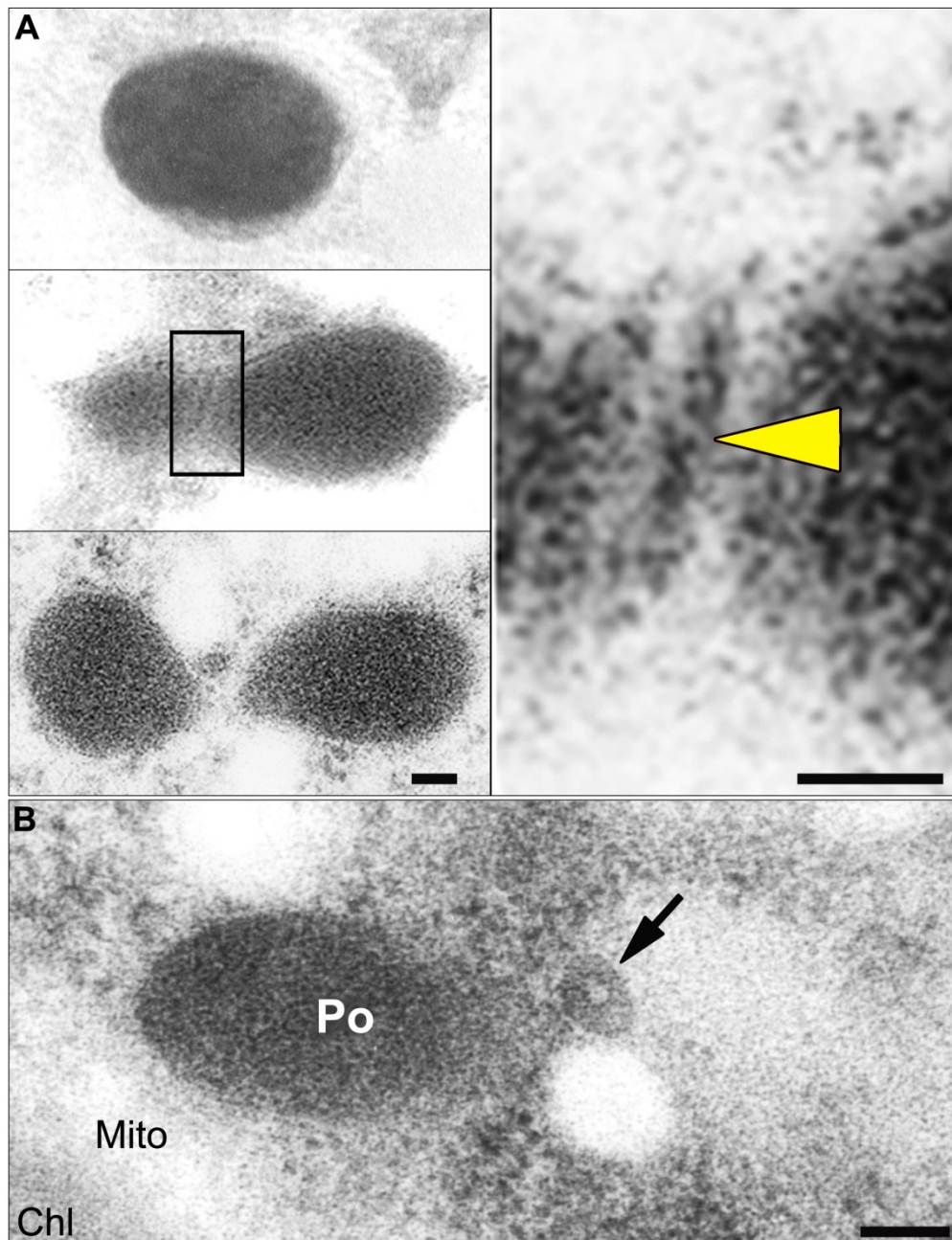
Fig. 2-18. Electron microscopic images showing dividing peroxisome after high-pressure freeze fixation.

(A) The edge of the POD machinery was visualized as a fine bar on the cytoplasmic side of the single membrane (yellow arrowhead) at the peroxisome division site. (B) Image perpendicular to the division site shows electron dense ring like structure (arrow) observed at the edge of the daughter peroxisome. Scale bars: 50 nm (A); 200 nm (B).
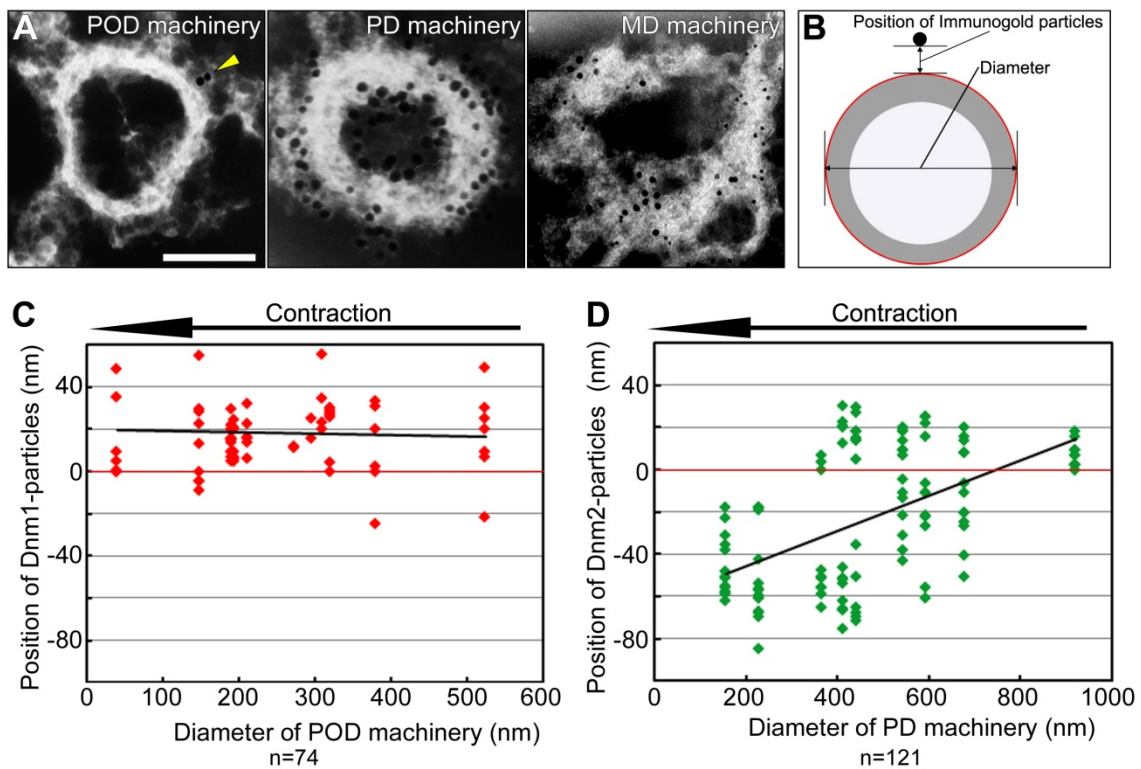
Fig. 2-19. Differences of distributions of dynamin between the POD and the PD machinery.

(A) Immunoelectron microscopic images of the POD machinery (15nm, anti-Dnm1), the PD machinery (15 nm, anti-Dnm2) and the MD machinery (15nm, Dnm1; 10 nm Mda1). (B) Schematic representation of the measurement line of the diameter and the position of immunogold particles. (C) Position of Dnm1-bound immunogold particles against the diameter of the POD machinery. (D) Position of Dnm2-bound immunogold particles against the diameter of the PD machinery. Scale bar: 200 nm.

POD machinery
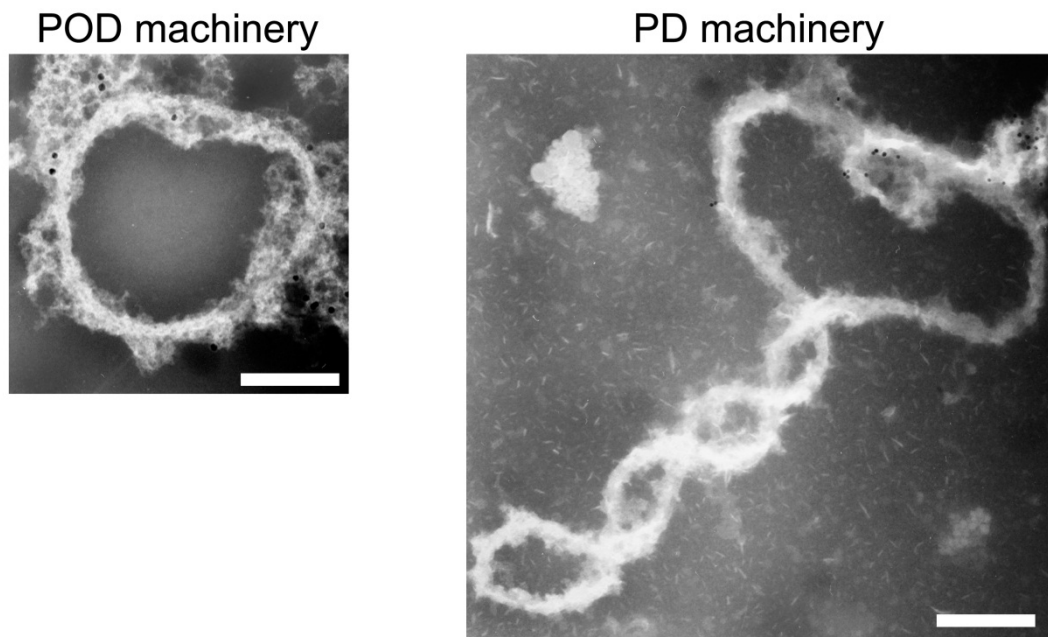
PD machinery

Fig. 2-20. POD machinery did not form supertwist structure.

POD machinery (15nm, anti-Dnm1) form circular structure while PD machinery can form supertwisted structure. Scale bar: 200 nm.
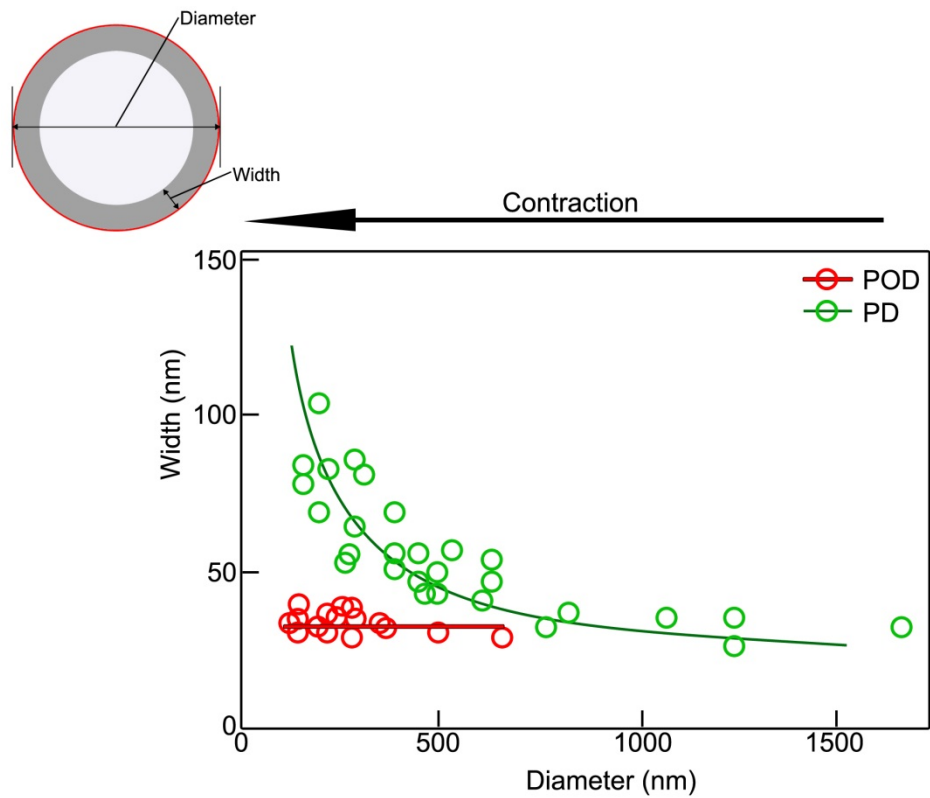
Fig. 2-21. Width of the filamentous ring of the POD machinery and PD machinery against its diameter.

  The width of the filamentous ring of the POD machinery (red) is constantly about 30 nm throughout contraction whereas the PD machinery (green) becomes wider during contraction.

Fig. 2-22. Isolated POD machinery arranged in order of contraction.

Immunoelectron microscopic images of POD machinery showed that clump of DB ring (yellow arrowhead) was remained and filamentous ring was disassembled at the final stage of the contraction. Immunogold particles (15 nm), Dnm1. Scale bar: 100 nm.

Fig. 2-23. Down-regulation of Dnm1.

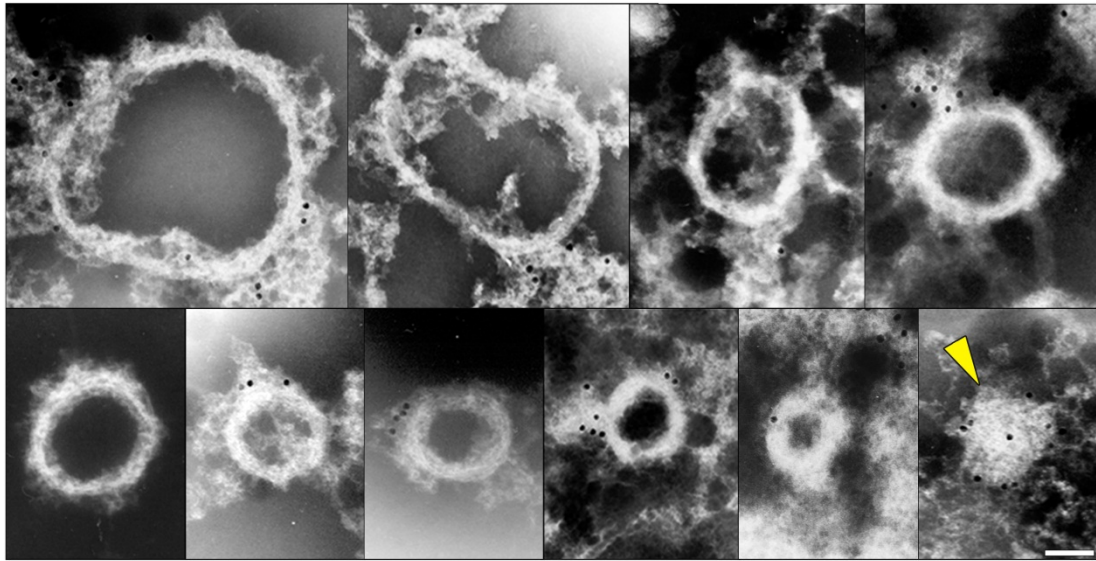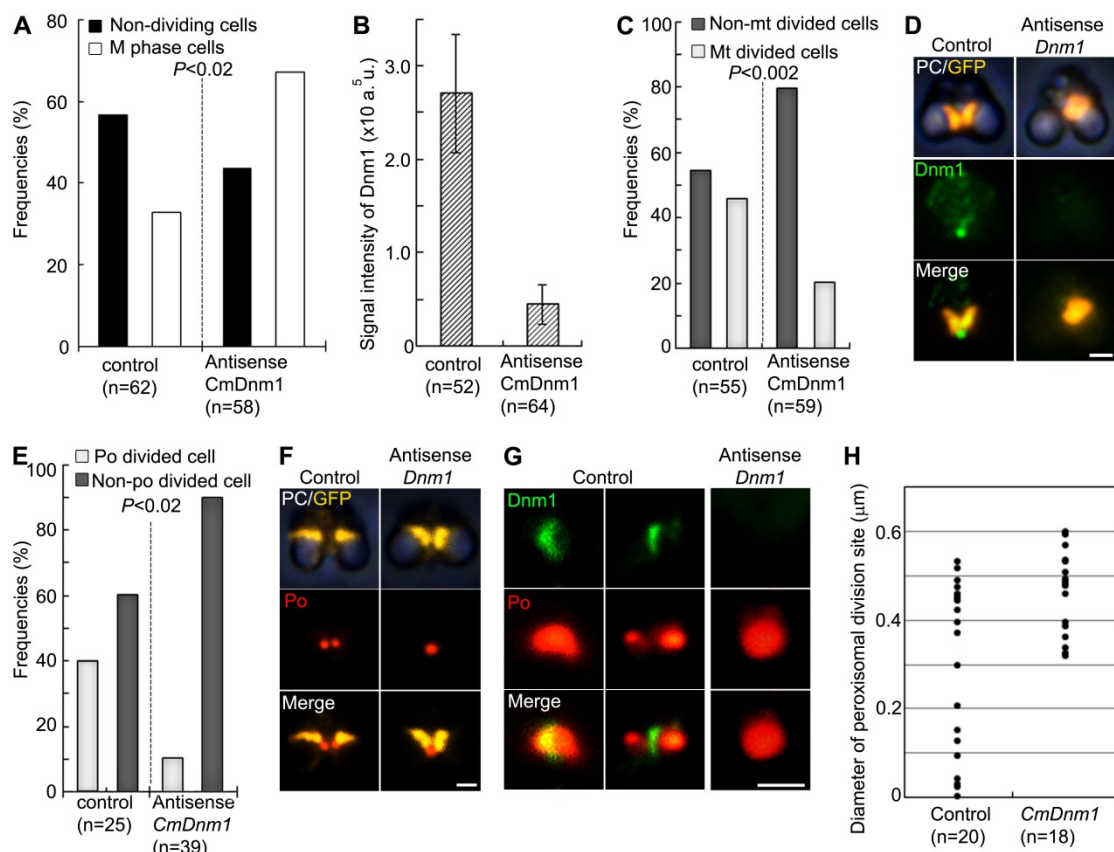(A) Frequencies of nondividing cells (interphase) and M phase cells. Nondividing cells are decreased, whereas M phase cells are increased, at 48 h after introduction of the antisense-Dnm1 DNA (P < 0.02 by Fisher's exact test). (B) The immunofluorescence intensity of the dynamin ring is decreased by the down-regulation. Data are means and SD (n > 50). (C) Down-regulation of Dnm1 inhibits mitochondrial division (n > 50; P < 0.002 by Fisher's exact test). (D) Phase-contrast and immunofluorescence images showing a dividing mitochondrion (GFP, yellow, anti-GFP) and Dnm1 (green) in control cells and a nondivided mitochondrion without dynamin in antisense-Dnm1 DNA-treated cells. (E) Cells with down-regulated Dnm1 show inhibited peroxisomal division, and the number of non–peroxisome-dividing cells is increased during late M phase (P < 0.02 by Fisher's exact test). Data are the frequencies of control and

83

antisense-Dnm1 DNA-treated cells with dividing peroxisomes (po) and nondividing peroxisomes (n > 25). (F) Phase-contrast and immunofluorescence images showing a dividing mitochondrion with a dividing peroxisome in control cells and a dividing mitochondrion with a nondividing peroxisome in antisense-Dnm1 DNA-treated cells. (G) Immunofluorescence images show a dividing peroxisome (red) with a dynamin ring (green) in control cells and a nondividing oval-shaped peroxisome without a dynamin ring in Dnm1-down-regulated cells. (H) Peroxisomal division in Dnm1–down-regulated cells stops at the early stage of contraction of the POD machinery. The data represent the diameters of the peroxisome division sites in control cells and antisense-Dnm1 DNA-treated cells. Scale bars: 1 μm.
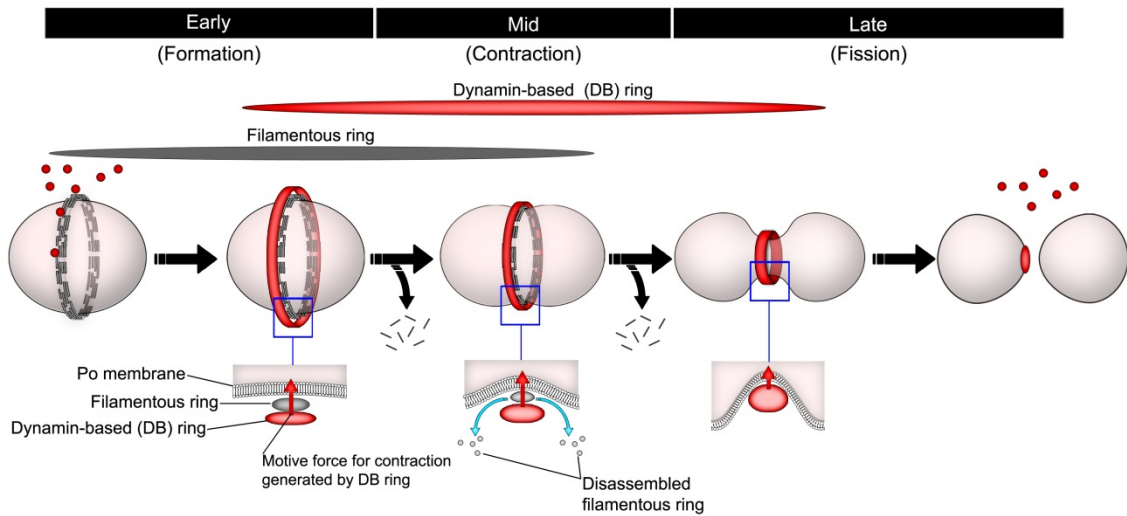
Fig. 2-24. **Working model of Dnm1 function in the POD machinery during the contraction and pinching off of peroxisomes at the division site.**

  The POD machinery consists of an outer dynamin-based ring (red) and an inner filamentous ring assembled on the cytosolic side of the peroxisome (Po) membrane. Dynamin-based ring (Dnm1 molecules and amorphous string) formed and encircles filamentous ring (Early). The dynamin-based ring generates contraction force for the POD machinery by sliding and constricts the filamentous ring at the division site of the peroxisome and partial digestion of the filamentous ring (Mid). The filamentous ring disassembles and then the single membrane bridge between the daughter peroxisomes is pinched off directly by the dynamin-based ring (Late). After division of the peroxisome, the dynamin molecules move to the cytosol.
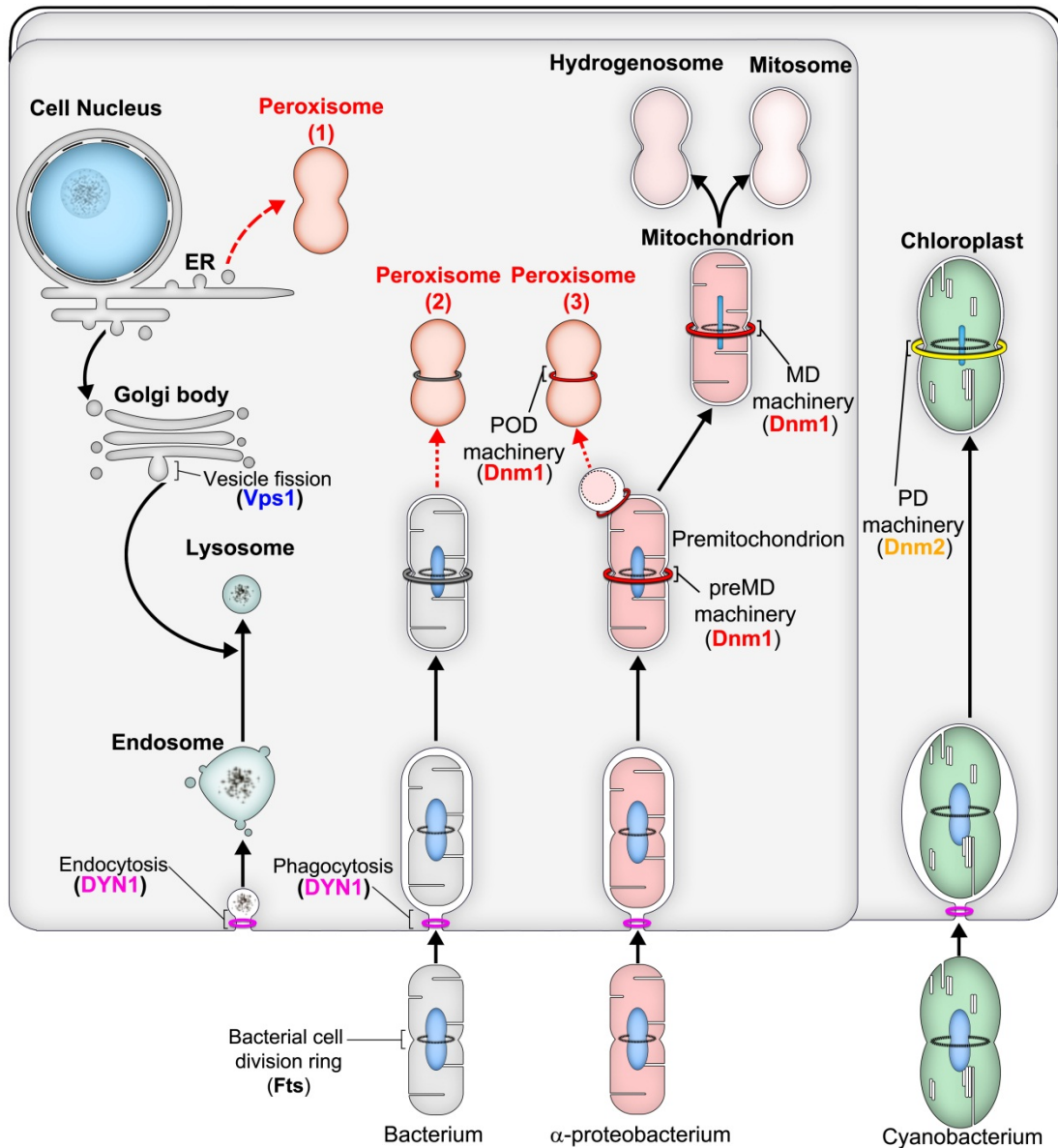
Fig. 2-25. S**chematic representation of origin and evolution of endosymbiotic organelles with an emphasis on organelle division machineries**.

  When an α-proteobacterium is engulfed by a eukaryotic cell containing cell-nuclear partners and becomes a mitochondrion, mitochondrial division comes to be regulated by the MD machineries (inner and outer dividing machineries). Mitosomes and hydrogenosomes may be generated from

mitochondria. When a cyanobacterium is engulfed by a eukaryotic cell containing a mitochondrion and become a chloroplast, chloroplast division come to be regulated by the PD machineries (inner and outer dividing machineries). It has been unknown whether peroxisome originates from premitochondrion which is the putative ancestor of mitochondira [peroxisome (3)] or unknown endosymbiotic bacterium [Peroxisome (2)].

Conclusion & perspectives

Structure of peroxisome (originally called microbodies) was discovered in 1954 using electron microscopy in a section of mouse kidney cells (Rhodin 1954). In 1966, peroxisomes were isolated from rat liver and catalase, an hydrogen peroxides degrading enzyme, in the matrix of peroxisomes (De Duve and Baudhuin 1966). Based on these findings, De Duve proposed the functional term "peroxisome", which gradually replaced the former morphological designation, "microbody". In addition, a fatty acid β-oxidation system in peroxisomes was discovered, which cooperates with mitochondria (Lazarow and De Duve 1976). According to their important role in lipid metabolism as well as in health and disease, peroxisomes are regarded as the one of the fundamental seven single- and double-membrane-bounded organelles (cell nucleus, mitochondria, chloroplast, ER, Golgi body, lysosome, peroxisome) in eukaryotic cells (Schrader and Yoon 2007; Kuroiwa et al. 2008; Imoto et al. 2011a). The discovery of the synthesis of peroxisomal matrix proteins on free polyribosomes in the cytoplasm (Goldman and Blobel 1978), like mitochondria and chloroplasts, led to the proposal of the "growth and division" model of peroxisome biogenesis with formation out of pre-existing organelles (Lazarow and Fujiki 1985). However multiperoxisomal organisms, such as yeasts, plants, and animals, contain irregularly shaped peroxisomes that divide randomly; the structure of division machinery (ring) that can divide peroxisomes had been remained elusive. In this thesis, the structure of peroxisome-dividing machinery (POD) has been revealed using isolated dividing peroxisome and genomic science of the primitive single celled red alga *Cyanidioschyzon merolae*.

First, microtubules and spindle poles mediated inheritance of peroxisome was revealed. α-tubulin was not organized during the G1 phase and organized to microtubules and spindle poles during M phase. Peroxisome division was controlled by spindle poles via interaction with daughter mitochondria. Inhibitions of microtubule organization induced delayed completion of peroxisome division, as a result, frequency of dividing peroxisome during the late M phase was increased. It enabled isolation of a large quantity of dividing peroxisomes (Imoto et al. 2010).

Next, dividing peroxisomes were isolated from *C. merolae* cells synchronized by light/dark cycles and oryzalin treatment. MALDI -TOF-MS analysis showed that dividing peroxisome fraction included one of the dynamin family members Dnm1 which was used for mitochondrial division. Immunofluorescence microscopy analysis showed that Dnm1 localized in this order: 1) Dnm1 localized in cytosol as dynamin patches during G1 phase, 2) Dnm1 recruited to mitochondrial division site from cytosol during early M phase, 3) dynamin patches appeared again in cytosol after the mitochondrial division, 4) Dnm1 recruited to peroxisomal division site from cytosol during the late M phase. Immunofluorescence and immunoelectron microscopy analysis showed that Dnm1 localized at the peroxisome division site in the isolated peroxisomes. When membrane was dissolved by detergent, ring-like structure appeared. The ring was POD machinery consists of dynamin-based (DB) ring and filamentous ring. POD machinery contracted from about 600 to 50 nm. DB ring contained Dnm1 and generated motive force for contraction, whereas filamentous ring did not contain Dnm1 but contained fragments of fine filament 4 nm in

diameter and disassembled during the contraction (Imoto et al. 2013). Identifications of the POD machinery supported the hypothesis that peroxisomes and mitochondria shared a common ancestor (Kuroiwa et al. 2008; Imoto et al. 2012). Inheritance of membrane-bounded organelles is classified into three units that the organelle partners accompanying with division: the cell nuclear unit, the mitochondrial unit and the chloroplast unit (Yagisawa et al. 2007; Fujiwara et al. 2010; Imoto et al. 2011a). Dnm1 family members were involved in both mitochondrial and peroxisomal division in animal, land plants, yeast (Bleazard al. 1999; Koch et al. 2003; Fujimoto et al. 2009) and the red alga *C. merolae* (Nishida et al. 2003; Imoto et al. 2013), while the cell nuclear unit and chloroplast unit used specific dynamins for each organelles (Praefcke and McMahon 2004; Miyagishima 2009).

This is the first evidence postulating that peroxisome division is performed by nano machinery consisting of an outer DB ring and an inner filamentous ring assembled on the cytosolic side of the peroxisome membrane. However, composition of DB ring and filamentous ring is still unknown. *C. merolae* represents an attractive experimental system to determine the components of intracellular structures due to the following reasons: (1) the 100%-complete genome sequence (16.5 Mb) of *C. merolae* has an extremely simple composition, with very few introns and low redundancy (Matsuzaki et al. 2004; Nozaki et al. 2007): (2) single- and double-membrane-bounded organelle divisions can be highly synchronized by light/dark cycles (Suzuki et al. 1994) and these organelles can be isolated with high purity (Yoshida et al. 2006, 2009; Yagisawa et al. 2009; Imoto et al. 2013). This is ideal for protein identification by

MALDI-TOF-MS, which is one of the most effective ways to identify proteins. Therefore, proteomic analysis of isolated POD machineries is thought to a useful strategy to determine unknown components of DB ring and filamentous ring.

DB ring was important structure for the contraction of the POD machinery and contained dynamin-like protein Dnm1 which was recruited from cytosol. To clarify the unknown components of DB ring which can recruit Dnm1 to the division site of peroxisome by using proteomic analysis will reveal more details of the molecular mechanism of the contraction of the POD machinery.

Filamentous ring including fine filaments about 4 nm in diameter was inner structure of the DB ring and thought to be a skeletal structure of the POD machinery. Electron microscopy analysis showed MD machineries were composed of a bundle of fine filaments (Yoshida et al. 2009), implying a structural similarity between the filamentous ring of the POD machinery and MD machinery. To determine the composition of these filaments by using proteomic analysis or other cytological techniques will reveal more details of the systems of peroxisomal division and origin of the single-membrane-bounded organelles.

References

Bleazard W, McCaffery JM, King EJ, Bale S, Mozdy A, Tieu Q, Nunnari J & Shaw JM (1999) The dynamin-related GTPase Dnm1 regulates mitochondrial fission in yeast. *Nat. Cell. Biol.* **1**:298–304.

Brown HR, Bouton JH, Rigsby L & Rigler M (1983) Photosynthesis of grass species differing in carbon dioxide fixation pathways. *Plant Physiol.* **71**:425-431.

Cavalier-Smith T (2000) Membrane heredity and early chloroplast evolution. *Trends Plant Sci.* **5**: 174-182

De Duve C & Baudhuin P (1966) Peroxisomes (microbodies and related particles). *Physiol. Rev.* **46**: 323-57

De Duve C (1969) The peroxisome: a new cytoplasmic organelle. *Proc. R. Soc. Lond., B, Biol. Sci.* **173**: 71–83.

De Duve C (1995) Vital dust: the origin and evolution of life on earth. Basic, New York.

Dolin MI (1961) Cytochromoindependent electron transport enzymes of bacteria. New York, Academic Press. **2**: 425-460.

Fang Y, Morrell JC, Jones JM & Gould SJ (2004) PEX3 functions as a PEX19 docking factor in the import of class I peroxisomal membrane

proteins. *J. Cell. Biol.* 164: 863-875.

Fujimoto M, Arimura S, Mano S, Kondo M, Saito C, Ueda T, Nakazono M, Nakano A, Nishimura M & Tsutsumi N (2009) Arabidopsis dynamin-related proteins DRP3A and DRP3B are functionally redundant in mitochondrial fission, but have distinct roles in peroxisomal fission. *Plant J.* **58**:388–400.

Fujiwara T, Misumi O, Tashiro K, Yoshida Y, Nishida K, Yagisawa F, Imamura S, Yoshida M, Mori T, Tanaka K & Kuroiwa T (2009a) Periodic gene expression patterns during the highly synchronized cell nucleus and organelle division cycles in the unicellular red alga *Cyanidioschyzon merolae*. *DNA Res.* **16**: 59–72.

Fujiwara T, Yoshida Y & Kuroiwa T (2009b) Synchronization of cell nuclear, mitochondrial and chloroplast divisions in the unicellular red alga *Cyanidioschyzon merolae*. *Cytologia* **74**, 1–2.

Gabaldón T, Snel B, van Zimmeren F, Hemrika W, Tabak H & Huynen MA (2006) Origin and evolution of the peroxisomal proteome. *Biology Direct* **1**:8

Gillham N W (1994) *Organelle Genes and Genomes*. Oxford University Press. Oxford, UK.

Goldman BM & Blobel G (1978) Biogenesis of peroxisomes: intracellular site of synthesis of catalase and uricase. *Proc. Natl. Acad. Sci. USA*

75:5066–5070

Gould SJ, Keller GA & Subramani S (1988) Identification of a peroxisomal targeting signal at the carboxy terminus of firefly luciferase. J. Cell. Biol. **105**: 2923-2931.

Gould SJ & Valle D (2000) Peroxisome biogenesis disorders: Genetics and cell biology. *Trends Genet* **16**:340–345.

Gray RH & Iglesia FA (1984) Quantitative Microscopy Comparison of Peroxisome Proliferation by the Lipid-Regulating Agent Gemfibrozil in Several Species. *Hepatology* **4**:520-530.

Hoepfner D, Schildknegt D, Braakman I, Philippsen P & Tabak HF (2005) Contribution of the Endoplasmic Reticulum to Peroxisome Formation. *Cell* **122**: 85–95.

Honda M & Hashimoto H (2007) Close association of centrosomes to distal ends of the microbody during its growth, division and partitioning in the green algae *Klebsormidium flaccidium*. *Protoplasma* **231**:127–135

Hunt, JE & Trelease RN (2004). Sorting pathway and molecular targeting signals for the Arabidopsis peroxin 3. *Biochem. Biophys. Res. Commun.* **314**: 586–596.

Imoto Y, Fujiwara T, Yohida Y, Kuroiwa H, Maruyama S & Kuroiwa T (2010) Division and segregation of cell nucleus, mitochondrion and

microbody mediated by centrosomes (mitotic spindle pole bodies) in the primitive red alga *Cyanidioschyzon merolae*. *Protoplasma* **241**: 63–74.

Imoto Y, Yagisawa F, Yoshida Y, Kuroiwa H & Kuroiwa T (2011a) The cell cycle, including the mitotic cycle and organelle division cycles, as revealed by cytological observations. *J. Electro. Micro.* **60**: 117-136

Imoto Y, Nishida K, Yagisawa F, Yoshida Y, Ohnuma M, Yoshida M, Fujiwara T, Kuroiwa H, Kawano S & Kuroiwa T (2011b) Involvement of elongation factor-1α in cytokinesis without actomyosin contractile ring in the primitive red alga *Cyanidioschyzon merolae*. *Cytologia.* **76**: 431-437

Imoto Y, Kuroiwa H, Ohnuma M, Kawano S & Kuroiwa T (2012) Identification of Peroxisome-Dividing Ring in *Cyanidioschyzon merolae* based on organelle partner hypothesis. *Cytologia.* **77**: 1–8

Imoto Y, Kuroiwa H, Yoshida Y, Ohnuma M, Fujiwara T, Yoshida M, Nishida K, Yagisawa F, Hirooka S, Miyagishima SY, Misumi O, Kawano S & Kuroiwa T (2013) Single-membrane-bounded peroxisome division revealed by isolation of dynamin-based machinery. *Proc. Natl. Acad. Sci. USA* **110**: 9583-9588.

Itoh R, Takahashi H, Toda K, Kuroiwa H & Kuroiwa T (1997) Checkpoint control on mitochondrial division in *Cyanidioschyzon merolae*. *Protoplasma* **196**:135–141

Hu J, Baker A, Bartel B, Linka N, Mullen RT, Reumann S & Zolman

BK (2012) Peroxisome Biogenesis and Function. *The Plant Cel,* **24**: 2279–2303.

Kobayashi S, Tanaka A & Fujiki Y (2007) Fis1, DLP1, and Pex11p coordinately regulate peroxisome morphogenesis. *Exp. Cell Res.* **313**: 1675-1686.

Koch A, Thiemann M, Grabenbauer M, Yoon Y, McNiven MA & Michael Schrader (2003) Dynamin-like protein 1 is involved in peroxisomal fission. *J. Biol. Chem.* **278**; 8597–8605.

Koch A, Schneider G, Lüers GH & Schrader M (2004) Peroxisome elongation and constriction but not fission can occur independently of dynamin-like protein 1. *J. Cell. Sci.* **117**:3995–4006.

Koch A, Yoon Y, Bonekamp NA, McNiven MA & Schrader M (2005) A role for Fis1 in both mitochondrial and peroxisomal fission in mammalian cells. *Mol. Biol. Cell.* **16**: 5077–5086.

Kornmann B, Currie E, Collins SR, Schuldiner M, Nunnari J, Weissman JS & Walter P (2009) An ER-Mitochondria Tethering Complex Revealed by a Synthetic Biology Screen. *Science* **325**: 477-481.

Kuroiwa T, Hizume M & Kawano S (1978) Studies on mitochondrial structure and function in Physarum polycephalum. *Cytologia* **43**:119–136

KuroiwaT (1982) Mitochondrial nuclei. *Int. Rev. Cytol.* **75**:1-59

Kuroiwa T, Nakamura S, Kawano S, Hizume M, Tho-e A, Miyakawa I & Sando N (1986) Cytological characterization of a synaptonemal complex-less nucleolar-organizing region on a bivalent in the bivalent of *Saccharomyces cerevisiae* using a video-intensified microscope system. *Exp. Cell. Res.* **165**:199–206

Kuroiwa T, Suzuki K, Itoh R, Toda K, Okeef T & Kawano S (1995) Mitochondria-dividing ring ultrastructural basis for the mechanisms of mitochondrial division in *Cyanidioschyzon merolae*. *Protoplasma* **186**:12–23

Kuroiwa T, Misumi O, Nishida K, Yagisawa F, Yoshida Y, Fujiwara T, Yoshida Y, Hirooka S & Kuroiwa H (2008) Structure, function, and origin of vesicle, mitochondrial and plastid division machineries with emphasis on dynamin rings and electron-dense rings. *Int. Rev. Cell Mol. Biol.* **271**: 97–141.

Kuravi K, Nagotu S, Krikken AM, Sjollema K, Deckers M, Erdmann R, Veenhuis M & van der Klei IJ (2006) Dynamin-related proteins Vps1p and Dnm1p control peroxisome abundance in *Saccharomyces cerevisiae*. *J. Cell. Sci.* **119**:3994–4001.

Lazarow PB & De Duve C (1976) A fatty acyl-CoA oxidizing system in rat liver peroxisomes; enhancement by clofibrate, a hypolipidemic drug. *Proc. Natl. Acad. Sci. USA* **73**:2043–2046

Lazarow PB & Fujiki Y (1985). Biogenesis of peroxisomes. *Ann. Rev. Cell Biol.* **1**: 489–530.

Li X & Gould SJ (2003) The dynamin-like GTPase DLP1 is essential for peroxisome division and is recruited to peroxisomes in part by PEX11. *J. Biol. Chem.* **278**: 17012–17020.

Margulis L (1970) *Origin of eukaryotic cells*. Yale University Press, New Haven, CT.

Matsuzaki M, Misumi O, Shin-i T, Maruyama S, Takahara M, Miyagishima S, Mori T, Nishida K, Yagisawa F, Nishida K, Yoshida Y, Nishimura Y, Nakao S, Kobayashi T, Momoyama Y, Higashiyama T, Minoda A, Sano M, Nomoto H, Oishi K, Hayashi H, Ohta F, Nishizaka S, Haga S, Miura S, Morishita T, Kabeya Y, Terasawa K, Suzuki Y, Ishii Y, Asakawa S, Takano H, Ohta N, Kuroiwa H, Tanaka K, Shimizu N, Sugano S, Sato N, Nozaki H, Ogasawara N, Kohara Y & Kuroiwa T (2004) Genome sequence of the ultra-small unicellular red alga Cyanidioschyzon merolae 10D. *Nature* **428**: 653–657.

Mita T, Kanbe T, Tanaka K & Kuroiwa T (1986) A ring structure around the dividing plane of the *Cyanidium caldarium* chloroplast. *Protoplasma* **130**: 211-213.

Miyagishima S, Itoh R, Toda K, Takahashi H, Kuroiwa H & Kuroiwa T (1998) Visualization of the microbody division in *Cyanidioschyzon merolae* with the fluorochrome brilliant sulfoflavin. *Protoplasma* **201**:115–

Miyagishima S, Itoh R, Toda K, Kuroiwa H & Kuroiwa T (1999a) Real-time analyses of chloroplast and mitochondrial division and differences in the behavior of their dividing rings during contraction. *Planta* **207**: 343–353.

Miyagishima S, Nishimura M, Itoh R, Toda K, Kuroiwa H & Kuroiwa T (1999b) Microbody proliferation and segregation cycle in the single microbody-alga *Cyanidioschyzon merolae*. *Planta* **208**: 326–336.

Miyagishima S, Nishida K, Mori T, Matsuzaki M, Higashiyama T, Kuroiwa H & Kuroiwa T (2003a) A plant-specific dynamin-related protein forms a ring at the chloroplast division site. *Plant Cell* **15**, 655–665.

Miyagishima S, Nishida K & Kuroiwa T (2003b) An evolutionary puzzle: chloroplast and mitochondrial division rings. *Trend Plant Sci.* **8**: 432-438.

Miyagishima SY, Kuwayama H, Urushihara H & Nakanishi H (2008) Evolutionary linkage between eukaryotic cytokinesis and chloroplast division by dynamin proteins. *Proc. Natl. Acad. Sci.* USA **105**:15202–15207.

Motley AM & Hettema EH (2007) Yeast peroxisomes multiply by growth and division. *J. Cell. Biol.* **178**:399–410.

Nishida K, Takahara M, Miyagishima S, Kuroiwa H, Matsuzaki M & Kuroiwa T (2003) Dynamic recruitment of Dynamin for final mitochondrial severance in a red alga. *Proc. Natl Acad. Sci. USA* **100**: 2146–2151.

Nishida K, Misumi O, Yagisawa F, Kuroiwa H, Nagata T & Kuroiwa T (2004) Triple immunofluorescent labeling of FtsZ, dynamin, and EF-Tu revealed a loose association between the inner and outer membrane mitochondrial division machinery in the red alga *Cyanidioschyzon merolae. J. Histochem. Cytochem.* **52**, 843-849.

Nishida K, Yagisawa F, Kuroiwa H, Nagata T & Kuroiwa T (2005) Cell cycle-regulated, microtubule-independent organelle division in *Cyanidioschyzon merolae. Mol. Biol. Cell.* **16**:2493–2502.

Nishida K, Yagisawa F, Kuroiwa H, Yoshida Y & Kuroiwa T (2007) WD40 protein Mda1 is purified with Dnm1 and forms a dividing ring for mitochondria before Dnm1 in *Cyanidioschyzon merolae. Proc. Natl Acad. Sci. USA* **104**, 4736–4741.

Nozaki H, Takano H, Misumi O, Terasawa K, Matuzaki M, Maruyama S, Nishida K, Yagisawa F, Yoshida Y, Fujiwara T, Takio S, Tamura K, Chung j-Chung, Nakamura S, Kuroiwa H, Tanaka K, Sato N & Kuroiwa T (2007) The first 100% complete eukaryotic genome sequences from the red alga *Cyanidioschyzon merolae* 10D. *BMC Biol.* **5**: 28.

Ohnuma M, Yokoyama T, Inoue T, Sekine Y & Tanaka K (2008)

Polyethylene glycol (PEG)-mediated transient gene expression in a red alga, *Cyanidioschyzon merolae* 10D. *Plant Cell Physiol.* **49**, 117–120.

Ohnuma M, Misumi O, Fujiwara T, Watanabe S, Tanaka K & Kuroiwa T (2009) Transient gene suppression in a red alga, *Cyanidooschyzon merolae* 10D. *Protoplasma* **236**: 107–112.

Pan R & Hu J (2011) The conserved fission complex on peroxisomes and mitochondria. *Plant Signal Behav* **6**:870–872.

Praefcke GJK & McMahon HT (2004) The dynamin superfamily: Universal membrane tubulation and fission molecules? *Nat. Rev. Mol. Cell. Biol.* 5:133–147.

Rhodin J (1954) Correlation of ultrastructural organization and function in normal and experimentally changed proximal tubule cells of the mouse kidney. Doctorate Thesis. Karolinska Institutet, Stockholm.

Schrader M & Yoon Y (2007) Mitochondria and peroxisomes: Are the 'big brother' and the 'little sister' closer than assumed? *Bioessays* **29**:1105–1114.

Suzuki K, Ehara T, Osafune T, Kuroiwa H, Kawano S & Kuroiwa T (1994) Cooperation behavior of mitochondria, chloroplast and their nuclei during the mitotic cycle in the ultra-microalga *Cyanidioschyzon merolae*. *Eur. J. Cell Biol.* **63**: 280–288.

Suzuki K, Kawazu T, Itoh R, Takahashi H & Kuroiwa T (1995) Cytokinesis by a contractile ring in the primitive red alga *Cyanidium caldarium* RK-1. *Eur. J. Cell. Bio* . **67**:170–178

Tabak HF, Murk JL, Braakman I & Geuze HJ (2003) Peroxisomes Start Their Life in the Endoplasmic Reticulum. *Traffic* **8**: 512-518.

Takahara M, Takahashi H, Matsunaga S, Miyagishima S, Takano H, Sakai A, Kawano S & Kuroiwa T (2000) A putative mitochondrial ftsZ gene is present in the unicellular primitive red alga *Cyanidioschyzon merolae*. *Mol. Gen. Genet.* **264**, 452–460.

Takahashi H, Takano H, Kawano S, Tohe A & Kuroiwa T (1996) Isolation, characterization and chromosomal mapping of an actin gene from the primitive red alga *Cyanidioschyzon merolae*. *Curr. Genet.* **28**: 484–490.

Tanaka A, Kobayashi S & Fujiki Y (2006) Peroxisome division is impaired in a CHO cell mutant with an inactivating point-mutation in dynamin-like protein 1 gene. *Exp. Cell. Res.* **312**:1671–1684.

Toda K, Takano H, Miyagishima S, Kuroiwa H & Kuroiwa T (1998) Characterization of a chloroplast isoform of serine acetyltransferase from the thermo-acidiphilic red alga *Cyanidioschyzone merolae. Biochim. Biophys. Acta.* **140**:72–84

Van Gestel K, Kohler RH & Verbelen JP (2002) Plant mitochondria move on F-actin, but their positioning in the cortical cytoplasm depends on

both F-actin and microtubules. *J. Exp. Bot.* **53**:659–667

Wiemer EAC, Wenzel T, Deerinck TJ, Ellisman MH & Subramani S (1997) Visualization of the peroxisomal compartment in living mammalian cells: dynamic behavior and association with microtubules. *J. Cell. Biol.* **136**:71–80

Yagisawa F, Nishida K, Kuroiwa H, Nagata T & Kuroiwa T (2007) Identification and mitotic partitioning strategies of vacuoles in the unicellular red alga Cyanidioschyzon merolae. *Planta* **226**: 1017–1029.

Yagisawa F, Nishida K, Yoshida M, Misumi O, Yoshida Y, Fujiwara T, Kuroiwa H & Kuroiwa T (2009) Major vacuolar proteins of the ultra-small unicellular red alga *Cyanidioschyzon merolae*. *Plant J.* **60**: 882–892.

Yagisawa F, Fujiwara T, Kuroiwa H, Nishida K, Imoto Y & Kuroiwa T (2012) Mitotic inheritance of endoplasmic reticulum in the primitive red alga *Cyanidioschyzon merolae*. *Protoplasma*. **249**: 1129-1135.

Yagisawa F, Fujiwara T, Ohnuma M, Nishida K, Imoto Y, Yoshida Y, Kuroiwa H & Kuroiwa T (2013) Golgi inheritance in the primitive red alga, *Cyanidioschyzon merolae*. *Protoplasma*. **250**: 943-8

Yasuda T, Kuroiwa T & Nagata T (1988) Induction of preferential DNA synthesis and replication of plastids in tobacco cultured cells by medium renewal. *Planta* **174**:235–241

Yoshida Y, Kuroiwa H, Misumi O, Nishida K, Nnamiya H, Yagisawa F, Fujiwara T, Kawamura F & Kuroiwa T (2006) Isolated chloroplast division machinery can actively constrict after stretching. *Science* **313**: 1435–1438.

Yoshida Y, Kuroiwa H, Hirooka S, Yoshida Y, Fujiwara T, Misumi O, Kawano S & Kuroiwa K (2009) Novel mitochondrial division protein ZED forms the inner complex structure of the mitochondrial division machinery with the ftsz ring as revealed by isolated mitochondrial division machineries. *Curr. Biol.* **19**: 1491–1497.

Yoshida Y, Kuroiwa H, Misumi O, Yoshida M, Ohnuma M, Fujiwara T, Yagisawa F, Hirooka S, Matsushita K, Kawano S & Kuroiwa T (2010) Plastid division is driven by glycoprotein PDR1 with polyglucan filaments. *Science* **329**: 949–953.

Yoshida Y, Fujiwara T, Imoto Y, Yoshida M, Ohnuma M, Hirooka S, Misumi O, Kuroiwa H & Kuroiwa T (2013) The kinesin-like protein TOP promotes Aurora localisation and induces mitochondrial, chloroplast and nuclear division. *J. Cell. Science* **126**:2392-400

Zhang XC & Hu JP (2008) FISSION1A and FISSION1B proteins mediate the fission of peroxisomes and mitochondria in Arabidopsis. *Mol. Plant.* **1**:1036–1047.